Physics – Uspekhi **48** (9) 887 – 902 (2005) ©2005 Uspekhi Fizicheskikh Nauk, Russian Academy of Sciences

REVIEWS OF TOPICAL PROBLEMS PACS numbers: 02.70.Uu, **71.35.–y**, **71.38.–k**, **74.72.–h**

Diagrammatic Monte Carlo method as applied to the polaron problems

A S Mishchenko

DOI: 10.1070/PU2005v048n09ABEH002632

Contents

Abstract. Numerical methods whereby exact solutions to the problem of a few particles interacting with one another and with several bosonic excitation branches are presented. The diagrammatic Monte Carlo method allows the exact calculation of the Matsubara Green function, and the stochastic optimization technique provides an approximation-free analytic continuation. In this review, results unobtainable by conventional methods are discussed, including the properties of excited states in the self-trapping phenomenon, the optical spectra of polarons in all coupling regimes, the validity range analysis of the Frenkel and Wannier approximations relevant to the exciton, and the peculiarities of photoemission spectra of a lattice-coupled hole in a Mott insulator.

1. Introduction

1.1 Basic concepts of the polaron

Historically, the first physical system to reveal strong coupling between a quasiparticle and its environment was the polaron — an electron interacting with lattice vibrations (for acquaintance, see Refs [1, 2]). As an electron moves through the crystal lattice, it changes its momentum each time it interacts with lattice excitation quanta (i.e., phonons) — a property to which there corresponds a single quantum number describing the state of a single structureless particle.

As increasingly complex objects were studied, the general physical significance of the polaron problem became clear. Depending on what the terms a 'particle', 'medium', and 'interaction' are taken to mean, a wide variety of diverse physical phenomena are covered by the polaron concept. This is nicely illustrated with an example of a hole moving in an antiferromagnet (a problem near-isomorphic to the one of a phonon polaron): the spin flip due to the motion of the hole is, in the spin wave approximation, equivalent to the hole changing its momentum due to the creation and absorption of spin waves (magnons) [3, 4]. An exciton – polaron considered in the intraband scattering approximation is another physical object which can be thought of as a structureless quasiparticle scattered by bosonic excitations. Intraband scattering by phonons leaves the wave function of electron – hole relative motion unchanged and so allows one to consider an exciton as a structureless single-particle excitation, which is equivalent to considering an ordinary phonon polaron with a renormalized coupling constant [5 – 7]. As reviewed in Ref. [8], a large number of rather exotic objects can be treated in terms of the classical polaron model of [1, 2].

Since L Landau [9], and H Frölich [10] pioneering work on the structureless particle model, the polaron concept has grown more sophisticated qualitatively, becoming relevant to ever more areas of condensed matter physics. A natural way to generalize the polaron concept was to allow the quasiparticle to have internal degrees of freedom which, together with the momentum, can change their quantum states when the quasiparticle interacts with medium excitations. Examples are the Jahn – Teller polaron whose coupling with lattice vibrations changes the quantum numbers of a degenerate electronic state [11], and the pseudo-Jahn – Teller polaron whose inelastic interaction with phonons can cause transitions between the quasiparticle's inner levels with close energies [12 – 14].

A S Mishchenko Russian Research Centre "Kurchatov Institute"
pl. Kurchatova 1, 123182 Moscow, Russian Federation
Tel. (7-095) 196 91 48. Fax (7-095) 943 00 74
E-mail: andry@kurm.polyn.kiae.su
CREST, Japan Science and Technology Agency (JST)
AIST, 1-1-1, Higashi, Tsukuba, Ibaraki 305-85-62, Japan
Tel. (81-29) 861 26 46. Fax (81-29) 851 79 15
E-mail: andry.mishenko@aist.go.jp

Received 17 February 2005
Uspekhi Fizicheskikh Nauk **175** (9) 925 – 941 (2005)
Translated by E G Strel'chenko; edited by A Radzig

A no less fundamental generalization of the polaron concept is a system of several interacting particles, each of which is a polaron. As these interact simultaneously with one another and with the environment, qualitatively new objects may form depending on the magnitude and sign of the coupling constants involved. For example, a 'bipolaronic' bound state between two repelling particles may form due to their effective phonon-mediated interaction [15–17]. On the other hand, the exciton-producing interaction of an electron and a hole with the quanta of crystal lattice vibrations potentially creates a wide variety of fundamentally different physical situations, including a trapped exciton, a bound pair formed by a trapped electron and a trapped hole, an electron weakly bound to a trapped hole, etc. [18, 19]. Impurities complicate model even further, due to the impurity potential interference with the polaron's own potential well induced by the lattice coupling [20].

1.2 Polaron model formulations

In its general formulation, the problem of a polaronic object is that of a system involving several particles (for simplicity, a two-particle system):

$$\widehat{H}_0^{\text{par}} = \sum_{\mathbf{k}} \varepsilon_a(\mathbf{k})\, a_{\mathbf{k}}^{\dagger} a_{\mathbf{k}} + \sum_{\mathbf{k}} \varepsilon_h(\mathbf{k})\, h_{\mathbf{k}} h_{\mathbf{k}}^{\dagger}\,, \tag{1}$$

where $a_{\mathbf{k}}$ and $h_{\mathbf{k}}$ are the annihilation operators, while $\varepsilon_a(\mathbf{k})$ and $\varepsilon_h(\mathbf{k})$ stand for the dispersion laws of the particles which interact with each other via an instantaneous nonretarded potential $\mathcal{U}(\mathbf{p},\mathbf{k},\mathbf{k}')$:

$$\widehat{H}_{\text{a-h}} = -N^{-1} \sum_{\mathbf{pkk}'} \mathcal{U}(\mathbf{p},\mathbf{k},\mathbf{k}')\, a_{\mathbf{p}+\mathbf{k}}^{\dagger}\, h_{\mathbf{p}-\mathbf{k}}^{\dagger}\, h_{\mathbf{p}-\mathbf{k}'}\, a_{\mathbf{p}+\mathbf{k}'} \tag{2}$$

(N is the number of particles in a system) and whose scattering is governed by the Hamiltonian

$$\widehat{H}_{\text{par-bos}} = \mathrm{i} \sum_{\varkappa=1}^{Q} \sum_{\mathbf{k},\mathbf{q}} (b_{\mathbf{q},\varkappa}^{\dagger} - b_{-\mathbf{q},\varkappa}) \big[\gamma_{aa,\varkappa}(\mathbf{k},\mathbf{q})\, a_{\mathbf{k}-\mathbf{q}}^{\dagger}\, a_{\mathbf{k}} + \gamma_{hh,\varkappa}(\mathbf{k},\mathbf{q})\, h_{\mathbf{k}-\mathbf{q}}^{\dagger}\, h_{\mathbf{k}} + \gamma_{ah,\varkappa}(\mathbf{k},\mathbf{q})\, h_{\mathbf{k}-\mathbf{q}}^{\dagger}\, a_{\mathbf{k}}\big] + \text{h.c.}\,, \tag{3}$$

where $\gamma_{[aa,ah,hh],\varkappa}$ are the corresponding coupling constants in creation and annihilation of quanta of one of the various bosonic elementary excitations in the medium, whose total number is Q:

$$\widehat{H}_{\text{bos}} = \sum_{\varkappa=1}^{Q} \sum_{\mathbf{q}} \omega_{\mathbf{q},\varkappa}\, b_{\mathbf{q},\varkappa}^{\dagger}\, b_{\mathbf{q},\varkappa}\,. \tag{4}$$

The formulation of the problem is even more complicated if each of the particles is allowed to have T internal quantum states:

$$\widehat{H}_0^{\text{PJT}} = \sum_{\mathbf{k}} \sum_{i=1}^{T} \epsilon_i(\mathbf{k})\, a_{i,\mathbf{k}}^{\dagger}\, a_{i,\mathbf{k}} \tag{5}$$

[$\epsilon_i(\mathbf{k})$ is the dispersion of a quasiparticle in its internal state i], transitions between which can be induced by the interaction

$$\widehat{H}_{\text{par-bos}} = \mathrm{i} \sum_{\varkappa=1}^{Q} \sum_{\mathbf{k},\mathbf{q}} \sum_{i,j=1}^{T} \gamma_{ij,\varkappa}(\mathbf{k},\mathbf{q}) (b_{\mathbf{q},\varkappa}^{\dagger} - b_{-\mathbf{q},\varkappa}) \times a_{i,\mathbf{k}-\mathbf{q}}^{\dagger} a_{j,\mathbf{k}} + \text{h.c.} \tag{6}$$

with some of the bosonic excitation branches.

In various simplified formulations of the problem, Eqns (1)–(6) govern a huge variety of physical problems. In the case of attractive potential $\mathcal{U}(\mathbf{p},\mathbf{k},\mathbf{k}') > 0$, formulas (1) and (2) describe exciton Hamiltonians for an effective static Coulomb potential with averaged dynamic screening [21, 22]. For the simplest case of particles coupled diagonally to just one phonon branch [$Q = 1$, $\gamma_{aa} = \gamma_{hh}$, and $\gamma_{ah} = 0$ in Eqn (3)], Eqns (1)–(4) describe a standard bipolaron [16, 17] or an exciton–polaron [7, 9, 22], depending on whether the potential is repulsive [$\mathcal{U}(\mathbf{p},\mathbf{k},\mathbf{k}') < 0$] or attractive [$\mathcal{U}(\mathbf{p},\mathbf{k},\mathbf{k}') > 0$]. Equations (4)–(6) apply to the simplest possible model of an exciton interacting with phonons — one in which only the two ($T = 2$) lowest states of relative motion are important (a 1D charge-transfer exciton, for example) — as well as to the problem of the Jahn–Teller polaron [all the ϵ_i's in Hamiltonian (5) are equal] and the pseudo-Jahn–Teller polaron. The problem of a hole in an antiferromagnet in the spin wave approximation is described by Eqns (4)–(6) with $Q = 1$ and $T = 1$, and if the hole interacts with phonons, then two bosonic branches should be taken into account, so that $Q = 2$ in equations (4) and (6). Finally, the classical problem of a structureless polaron coupled to a single phonon branch is covered by the simplest nontrivial set of the particle

$$\widehat{H}_{\text{par}} = \sum_{\mathbf{k}} \epsilon(\mathbf{k})\, a_{\mathbf{k}}^{\dagger} a_{\mathbf{k}}\,, \tag{7}$$

phonon

$$\widehat{H}_{\text{ph}} = \sum_{\mathbf{q}} \omega_{\mathbf{q}} b_{\mathbf{q}}^{\dagger} b_{\mathbf{q}}\,, \tag{8}$$

and interaction

$$\widehat{H}_{\text{int}} = \sum_{\mathbf{k},\mathbf{q}} V(\mathbf{k},\mathbf{q}) (b_{\mathbf{q}}^{\dagger} - b_{-\mathbf{q}})\, a_{\mathbf{k}-\mathbf{q}}^{\dagger} a_{\mathbf{k}} + \text{h.c.} \tag{9}$$

Hamiltonians.

The essential point here is that, except for the simplest limiting cases, none of the above problems is amenable to an analytical solution. Nor, as discussed in detail in the subsequent sections, can conventional numerical approaches (such as variational methods, exact diagonalization schemes, or renormalization group techniques) provide complete and accurate information about the ground and excited states of a macroscopic system. Section 2 of this review presents two newly developed methods — the diagrammatic Monte Carlo (or DMC) method for exactly calculating Green's functions [24–32] and the stochastic optimization (SO) [26] technique — whose combination allows us to find exact (i.e., approximation-free) numerical solutions to the problems discussed in this section. The reader not interested in the methods as such can read Section 2.1 and then skip to Section 3 for the results obtained with these approaches. Section 3 analyzes the results on systems and phenomena, most of which have never before been treated without employing essential approximations and whose interpretation, as a consequence, was not entirely flawless. These include self-trapping, relaxed excited state, the end point of the polaron spectrum, and hole motion in an antiferromagnet under conditions of a strong electron–phonon interaction.

2. Diagrammatic Monte Carlo method and the stochastic optimization technique for constructing analytic continuation

2.1 Informative characteristics of the polarons

To gain adequate information on the ground and excited states of a system, it suffices to calculate the imaginary-time Green function (GF) in the Matsubara representation and then to analytically continue it to real frequencies [33, 34]. For two particles interacting with a boson field [see Eqns (1)–(4)], an informative quantity is the two-particle GF [29, 30]

$$G_{\mathbf{k}}^{\mathbf{pp}'}(\tau) = \langle \mathrm{vac} \mid a_{\mathbf{k}+\mathbf{p}'}(\tau)\, h_{\mathbf{k}-\mathbf{p}'}(\tau)\, h^{\dagger}_{\mathbf{k}-\mathbf{p}} a^{\dagger}_{\mathbf{k}+\mathbf{p}} \mid \mathrm{vac}\rangle\,, \tag{10}$$

where $h_{\mathbf{k}-\mathbf{p}}(\tau) = \exp(\widehat{H}_\tau)\, h_{\mathbf{k}-\mathbf{p}} \exp(-\widehat{H}_\tau)$, and $\tau > 0$. In the exciton–polaron case, the vacuum state $|\,\mathrm{vac}\rangle$ is one with the conduction band empty and the valence band full, whereas for the bipolaron problem this corresponds to a system with no particles (or no holes). For the simplified problem of a particle with an internal structure defined by two energy levels (4)–(6), an informative quantity is the one-particle matrix GF [27, 30]

$$G_{\mathbf{k},ij}(\tau) = \langle \mathrm{vac} \mid a_{i,\mathbf{k}}(\tau)\, a^{\dagger}_{j,\mathbf{k}} \mid \mathrm{vac}\rangle, \qquad i, j = 1, 2\,. \tag{11}$$

For the simplest problem of a structureless polaron [see Eqns (7)–(9)], matrix (11) reduces to a single-particle GF

$$G_{\mathbf{k}}(\tau) = \langle \mathrm{vac} \mid a_{\mathbf{k}}(\tau)\, a^{\dagger}_{\mathbf{k}} \mid \mathrm{vac}\rangle\,. \tag{12}$$

Important information about the physical response (for example, the optical absorption) of the polaron system can also be obtained from the current–current correlation function $\langle J_\beta(\tau)\, J_\delta\rangle$, where β and δ are Cartesian subscripts.

What the GF $G_{\mathbf{k}}(\tau)$ means physically becomes clear from the Lehmann representation [33, 34]:

$$G_{\mathbf{k}}(\tau) = \int_0^\infty L_{\mathbf{k}}(\omega) \exp(-\omega\tau)\, \mathrm{d}\omega\,, \tag{13}$$

$$L_{\mathbf{k}}(\omega) = \sum_{\nu} \delta\big(\omega - E_\nu(\mathbf{k})\big) \big|\langle \nu | a^{\dagger}_{\mathbf{k}} \mid \mathrm{vac}\rangle\big|^2\,. \tag{14}$$

Here, $\{|\nu\rangle\}$ is the complete set of eigenstates of the total Hamiltonian $\widehat{H}$ of the system in the sector of a given momentum $\mathbf{k}$, i.e., $H|\nu(\mathbf{k})\rangle = E_\nu(\mathbf{k})|\nu(\mathbf{k})\rangle$. It should be noted that, for simplicity, Eqns (13), (14) are presented for the case of one particle at zero temperature; general expressions can be found in the review article [35]. The Lehmann spectral function $L_{\mathbf{k}}(\omega)$ has poles (sharp peaks) at frequencies corresponding to the stable (metastable) states of the particle. For example, if for a given $\mathbf{k}$ there exists a stable state with energy $E(\mathbf{k})$, the Lehmann function can be presented in the form

$$L_{\mathbf{k}}(\omega) = Z^{(\mathbf{k})} \delta(\omega - E(\mathbf{k})) + \ldots\,. \tag{15}$$

At zero temperature, the lowest state in the sector of a given momentum $\mathbf{k}$ stands out as special in that the GF asymptotics

$$G_{\mathbf{k}}(\tau \gg \max\big[\omega^{-1}_{\mathbf{q},\varkappa}\big]) \to Z^{(\mathbf{k})} \exp\big(-E_{\mathrm{g.s.}}(\mathbf{k})\,\tau\big) \tag{16}$$

'projects' the energy $E_{\mathrm{g.s.}}(\mathbf{k})$ and $Z^{(\mathbf{k})}$-factor of this state. The asymptotic behavior of the GFs given by Eqns (10)–(12) or of those considered in Refs [26, 29] provides even more detailed information on the lowest state for a given momentum $\mathbf{k}$. For example, for a particle's ground state wave function

$$\Psi_{\mathrm{g.s.}}(\mathbf{k}) = \sum_{i=1}^{T} \sum_{n=0}^{\infty} \sum_{\mathbf{q}_1 \ldots \mathbf{q}_n} \theta_i(\mathbf{k}; \mathbf{q}_1, \ldots, \mathbf{q}_n) \times c^{\dagger}_{i,\mathbf{k}-\mathbf{q}_1 \ldots -\mathbf{q}_n} b^{\dagger}_{\mathbf{q}_1} \ldots b^{\dagger}_{\mathbf{q}_n} \mid \mathrm{vac}\rangle\,, \tag{17}$$

the important characteristics are the unity-normalized ($\sum_{n=0}^{\infty} Z^{(\mathbf{k})}(n) \equiv 1$) partial n-phonon contributions

$$Z^{(\mathbf{k})}(n) \equiv \sum_{i=1}^{T} \sum_{\mathbf{q}_1 \ldots \mathbf{q}_n} \big|\theta_i(\mathbf{k}; \mathbf{q}_1, \ldots, \mathbf{q}_n)\big|^2 \tag{18}$$

and the average number of photons

$$\langle N\rangle \equiv \Big\langle \Psi_{\mathrm{g.s.}}(\mathbf{k}) \Big| \sum_{\mathbf{q}} b^{\dagger}_{\mathbf{q}} b_{\mathbf{q}} \Big| \Psi_{\mathrm{g.s.}}(\mathbf{k}) \Big\rangle = \sum_{n=1}^{\infty} n Z^{(\mathbf{k})}(n)\,, \tag{19}$$

both of which can be obtained from the analysis of the n-phonon GFs [26]

$$G_{\mathbf{k}}(n, \tau; \mathbf{q}_1, \ldots, \mathbf{q}_n) = \langle \mathrm{vac}|\, b_{\mathbf{q}_n}(\tau) \ldots b_{\mathbf{q}_1}(\tau)\, a_{\mathbf{p}}(\tau)\, a^{\dagger}_{\mathbf{p}} b^{\dagger}_{\mathbf{q}_1} \ldots b^{\dagger}_{\mathbf{q}_n} |\,\mathrm{vac}\rangle\,,$$
$$\mathbf{p} = \mathbf{k} - \sum_{j=1}^{n} \mathbf{q}_j\,. \tag{20}$$

Another example is provided by the wave function of relative motion of the exciton in the lowest state $E_{\mathrm{g.s.}}(\mathbf{k})$ for a given momentum:

$$\Psi_{\mathrm{g.s.}}(\mathbf{k}) = \sum_{\mathbf{p}} \xi_{\mathbf{kp}}(\mathrm{g.s.})\, a^{\dagger}_{\mathbf{k}+\mathbf{p}}\, h^{\dagger}_{\mathbf{k}-\mathbf{p}} |\,\mathrm{vac}\rangle\,, \tag{21}$$

whose amplitudes $\xi_{\mathbf{kp}}(\mathrm{g.s.})$ can be obtained from the asymptotics of the GF (10):

$$G_{\mathbf{k}}^{\mathbf{p}=\mathbf{p}'}(\tau \to \infty) = |\xi_{\mathbf{kp}}\,(\mathrm{g.s.})|^2 \exp(-E_{\mathrm{g.s.}}(\mathbf{k})\tau) \tag{22}$$

for equal values of the relative momenta, namely, $\mathbf{p} = \mathbf{p}'$ [29].

Information about the excited states can be obtained from the solution of the Fredholm equation $G_{\mathbf{k}}(\tau) = \widehat{\mathcal{F}}\big[L_{\mathbf{k}}(\omega)\big]$ (13):

$$L_{\mathbf{k}}(\omega) = \widehat{\mathcal{F}}^{-1}_{\omega}\big[G_{\mathbf{k}}(\tau)\big]\,. \tag{23}$$

Equation (13) governs quite a general relation between the imaginary-time GF (or the correlation function) and the spectral properties of the system. For example, in the case of a momentum-independent optical matrix element, the coefficient of light absorption by excitons, $\mathcal{I}(\omega)$, can also be obtained [29] by inverting the Fredholm equation for the liner combination of the GFs given by Eqn (10):

$$\mathcal{I}(\omega) = \widehat{\mathcal{F}}^{-1}_{\omega}\Big[\sum_{\mathbf{pp}'} G_{\mathbf{k}=0}^{\mathbf{pp}'}(\tau)\Big]\,, \tag{24}$$

while the real part of the optical conductivity $\sigma_{\beta\delta}(\omega)$ is, according to Ref. [31], expressed in terms of the current–current correlation function $\langle J_\beta(\tau) J_\delta\rangle$ as

$$\sigma_{\beta\delta}(\omega) = \frac{\pi}{\omega}\, \widehat{\mathcal{F}}^{-1}_{\omega} \langle J_\beta(\tau)\, J_\delta\rangle\,. \tag{25}$$

In most cases, the GFs (10)–(12) and the correlation function $\langle J_\beta(\tau) J_\delta \rangle$ cannot be determined analytically, and the DMC method is the only one applicable to a macroscopic system (to be discussed in detail in Section 2.2). The attempt [35, 36] to invert the Fredholm equation (13) by the standard maximum entropy (ME) technique proved to be an ill-posed problem and failed to produce satisfactory results because of sharp peaks and smooth incoherent parts coexisting in typical quasiparticle spectra (see the work [35] for a review of the ME technique). In these cases, the recently developed [26] stochastic optimization (SO) method can be usefully applied, whose description is given in Section 2.3.

2.2 Diagrammatic Monte Carlo method

The DMC method offers a systematic-error-free algorithm for calculating GFs (10)–(12) using the Feynman diagrammatic expansion for the imaginary-time Matsubara Green function. What follows is a detailed exposition of the fundamentals of the DMC method as applied to the simplest problem of calculating GF (12) for a single structureless polaron (7)–(9); generalizations to more complex cases can be found in Refs [27–32]. The DMC method is based on the expansion of the GF in the interaction representation:

$$G_{\mathbf{k}}(\tau) = \left\langle \mathrm{vac} \middle| T_\tau \left[a_{\mathbf{k}}(\tau)\, a^\dagger_{\mathbf{k}}(0) \times \exp\left(-\int_0^\infty \widehat{H}_{\mathrm{int}}(\tau')\, \mathrm{d}\tau' \right) \right] \middle| \mathrm{vac} \right\rangle_{\mathrm{con}}, \qquad \tau > 0\,. \tag{26}$$

Here, T_τ is the chronological ordering operator, $|\mathrm{vac}\rangle$ is the no-particle no-phonon vacuum state, and $\widehat{H}_{\mathrm{int}}$ is the interaction Hamiltonian as given by Eqn (9). The exponential symbol implies a Taylor expansion, an operation which leads to multiple integrals over the internal variables $\{\tau'_1, \tau'_2, \ldots\}$. All operators depending on imaginary time τ are defined in the interaction representation

$$\widehat{A}(\tau) = \exp\left[\tau(\widehat{H}_{\mathrm{par}} + \widehat{H}_{\mathrm{ph}})\right] \widehat{A} \exp\left[-\tau(\widehat{H}_{\mathrm{par}} + \widehat{H}_{\mathrm{ph}})\right].$$

The subscript 'con' in Eqn (26) is meant to indicate that the expansion includes only connected diagrams, i.e., only those expansion terms in which none of the integrals over the internal imaginary-time variables $\{\tau'_1, \tau'_2, \ldots\}$ can be represented by a separate factor.

Using the Wick theorem, a matrix element of the product of chronological ordering operators is expressed as the sum of the products of matrix elements of pairs of operators, reducing expansion (26) to an infinite sum of terms in the form of multiple integrals in which the number of integrand variables increases to infinity:

$$G_{\mathbf{k}}(\tau) = \sum_{m=0,2,4\ldots}^{\infty} \sum_{\xi_m} \int \mathcal{D}_m^{(\xi_m)}\left(\tau; \{x'_1, \ldots, x'_m\}\right) \mathrm{d}x'_1 \ldots \mathrm{d}x'_m\,. \tag{27}$$

In this formula, ξ_m numbers various diagrams with the same order m. The term with $m = 0$ is the GF $G^{(0)}_{\mathbf{k}}(\tau)$ of a noninteracting particle. The integrands $\mathcal{D}_m^{(\xi_m)}\left(\tau; \{x'_1, \ldots, x'_m\}\right)$ are, for any order, the product of the GFs $G^{(0)}_{\mathbf{k}}(\tau_2 - \tau_1) = \exp\left[-\epsilon(\mathbf{k})(\tau_2 - \tau_1)\right]$ and $D^{(0)}_{\mathbf{q}}(\tau_2 - \tau_1) = \exp\left[-\omega_{\mathbf{q}}(\tau_2 - \tau_1)\right]$, $\tau_2 > \tau_1$, known for the noninteracting system of a particle and phonons, times the interaction vertices $V(\mathbf{k}, \mathbf{q})$. For the DMC and other Monte Carlo methods to be successful, it is desirable that Eqn (27) comprised all terms of the same sign — which dictates using the Matsubara representation because in any other representation the expansion terms vary in sign and sometimes are complex numbers.

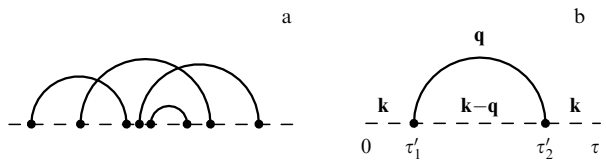

Figure 1. (a) Typical diagram contributing to expansion (27). (b) A second-order diagram.

The weight computation rules for the diagrammatic terms of the series $\mathcal{D}_m^{(\xi_m)}\left(\tau; \{x'_1, \ldots, x'_m\}\right)$ can be defined in explicit form for a term of any topology and order. The GFs $G^{(0)}_{\mathbf{k}}(\tau_2 - \tau_1)$ of a noninteracting particle with the corresponding momentum and times are assigned to the horizontal line of the propagator, whereas to the GF of noninteracting phonons $D^{(0)}_{\mathbf{q}}(\tau_2 - \tau_1)$ (times the product of the corresponding vertices $V(\mathbf{k}', \mathbf{q}) V^*(\mathbf{k}'', \mathbf{q})$) the arch of the phonon propagator is put into correspondence (Fig. 1a). For example, the weight of the second-order term (Fig. 1b) is given by

$$\mathcal{D}_2(\tau; \{\tau'_2, \tau'_1, \mathbf{q}\}) = \left|V(\mathbf{k}, \mathbf{q})\right|^2 D^{(0)}_{\mathbf{q}}(\tau'_2 - \tau'_1)\, G^{(0)}_{\mathbf{k}}(\tau'_1) \times G^{(0)}_{\mathbf{k}-\mathbf{q}}(\tau'_2 - \tau'_1)\, G^{(0)}_{\mathbf{k}}(\tau - \tau'_2)\,. \tag{28}$$

The DMC process constitutes a numerical procedure based on the Metropolis principle [37, 38], which evaluates different diagrams by sampling in the space of parameters $(\tau, m, \xi_m, \{x_m\})$ and collects statistics on the values of the external variable τ in such a way that the result converges to the exact value of the GF $G_{\mathbf{k}}(\tau)$. This is akin to using the Monte Carlo method for calculating the dependence of a multidimensional integral on an external parameter — with the crucial difference, however, that the number of integration variables in expansion (27) is a varying quantity. Although the sum of series (27) is obtained in a single process [24], the procedure is simpler to describe if one starts from an algorithm for calculating the dependence on the external parameter τ for one of the terms in the expansion $\mathcal{D}_m^{(\xi_m)}(\tau; \{x'_1, \ldots, x'_m\})$.

Starting from a certain initial set of parameters, $\{\tau; \{x'_1, \ldots, x'_m\}\}$, at each step of the process one of the parameters (τ or the internal variable x'_l) randomly selected from the others is subjected to the replacement $x_l^{\mathrm{old}} \to x_l^{\mathrm{new}}$, which is either accepted or rejected according to the Metropolis algorithm. After performing a sufficient number of steps that affect all the parameters $\{\tau; \{x'_1, \ldots, x'_m\}\}$ without exception, the statistics of the outer variable τ tend toward the exact dependence of the expansion term in formula (27) on τ. The new value of the parameter $x_l^{(\mathrm{new})} = \widehat{S}^{-1}(R)$, where $\widehat{S}^{-1}(R)$ is the solution of the integral equation

$$\int_{x_l^{\min}}^{x_l^{\mathrm{new}}} W(x')\, \mathrm{d}x' = R\,, \tag{29}$$

is generated using the random number $R \in [0, 1]$.

The distribution function $W(x_l)$ entering this equation is normalized to unity over the range $x_l^{\min} < x_l < x_l^{\max}$ and,

while otherwise arbitrary, is subject to two restrictions. First, it should not lead to new parameters x_l^{new} which violate the topology of the given expansion term. For example, the internal time τ_1' in Fig. 1b must fall in the range $[x^{\min} = 0, x^{\max} = \tau_2']$. Second, the distribution should be nonzero everywhere in its definition domain consistent with the topology of the diagram, because to obtain the exact result the DMC sampling must cover the entire region of allowed parameters (the ergodicity property). At each step, the decision on the change $x_l^{\text{old}} \to x_l^{\text{new}}$ is made after calculating the ratio

$$M = \frac{\mathcal{D}_m^{(\xi_m)}(\tau; \{x_1', \ldots, x_l^{\text{new}}, \ldots, x_m'\})/W(x_l^{\text{new}})}{\mathcal{D}_m^{(\xi_m)}(\tau; \{x_1', \ldots, x_l^{\text{old}}, \ldots, x_m'\})/W(x_l^{\text{old}})} \tag{30}$$

with the probability

$$P_{\text{acc}} = \begin{cases} M, & \text{or} \quad M < 1\,, \\ 1, & \text{or} \quad M \geqslant 1\,. \end{cases} \tag{31}$$

Assuming for simplicity a uniform distribution $W = \text{const} = (x_l^{\max} - x_l^{\min})^{-1}$, it can be seen that the probability of occurrence of any combination of parameters in the DMC procedure is proportional to the value of the function $\mathcal{D}$. In the practical implementation of the method, the distribution $W(x_l^{\text{new}})$ should be as close as possible to the true one specified by the function $\mathcal{D}_m^{(\xi_m)}(\tau; \{x_1', \ldots, x_l^{\text{new}}, \ldots, x_m'\})$. In the limiting case, when the two distributions are the same and the ratio M equals unity, all the parameter changes are accepted, maximizing the speed and efficiency of the sampling for parameters which are most representative in the diagram.

In evaluating diagrams of different orders by sampling, it is sufficient to use two types of mutually reciprocal transformations. The first transformation, $\mathcal{A}$, turns the diagram $\mathcal{D}_m^{(\xi_m)}(\tau; \{x_1', \ldots, x_m'\})$ into a higher-order diagram $\mathcal{D}_{m+2}^{(\xi_{m+2})}(\tau; \{x_1', \ldots, x_m'; \mathbf{q}', \tau', \tau''\})$ which possesses an additional phonon arch and connects certain points τ' and τ'' by a phonon propagator with momentum $\mathbf{q}'$. In this case, the weight ratio

$$\frac{\mathcal{D}_{m+2}^{(\xi_{m+2})}\big(\tau; \{x_1', \ldots, x_m'; \mathbf{q}', \tau', \tau''\}\big)}{\mathcal{D}_m^{(\xi_m)}\big(\tau; \{x_1', \ldots, x_m'\}\big)}$$

is not dimensionless because the expressions $\mathcal{D}_{m+2}^{(\xi_{m+2})}\,\mathrm{d}\mathbf{q}\,\mathrm{d}\tau'\,\mathrm{d}\tau''$ and $\mathcal{D}_m^{(\xi_m)}$ possess the same dimension. However, in the $\mathcal{A}$ operation the values of the parameters of the new phonon propagator are suggested with probability $W(\mathbf{q}', \tau', \tau'')\,\mathrm{d}\mathbf{q}\,\mathrm{d}\tau'\,\mathrm{d}\tau''$ [which is determined by the unity-normalized distribution function $W(\mathbf{q}', \tau', \tau'')$], and acting as a dimensionless parameter is the quantity

$$M = \frac{\mathcal{D}_{m+2}^{(\xi_{m+2})}\big(\tau; \{x_1', \ldots, x_m;\ \mathbf{q}', \tau', \tau''\}\big)}{\mathcal{D}_m^{(\xi_m)}\big(\tau; \{x_1', \ldots, x_m\}\big)\,W(\mathbf{q}', \tau', \tau'')}\,. \tag{32}$$

The opposite procedure $\mathcal{B}$ employs the inverse ratio M^{-1} [24, 26].

The above diagram transformations are local in the sense that they are independent on the structure of the diagram as a whole, so that neither the rules used nor the transformation processing time change as the order of the diagram is increased. The DMC method does not imply any explicit 'cut off' of the order of the terms in series (27) to account for finite computer memory. Even when taking summation for strongly coupled systems, typically with a very large number of phonon propagators N_{ph} in the contributing diagrams, the finite memory effect can be made negligible. Clearly, from the central limit theorem it follows that the number of phonon propagators in representative diagrams adheres to a Gaussian distribution with a maximum at point $\bar{N}_{\text{ph}}$ and with half-width of order $(\bar{N}_{\text{ph}})^{1/2}$ [39]. Thus, with a memory reserve at least twice what is necessary for describing diagrams of order $\bar{N}_{\text{ph}}$, system fluctuations will no reach the size of diagrams that are beyond the reserve.

An extension of the above technique to the case of the exciton [see Eqns (1), (2)] is given in Ref. [29], and its application to the pseudo-Jahn–Teller polaron [defined by Eqns (4)–(6)] is discussed in Ref. [27]. Paper [31] modifies the method to calculate the current–current correlation function of polarons, and work [32] treats the case in which interaction with several bosonic excitation branches takes place. Finally, further modifications of the method are reviewed in Ref. [30].

2.3 Stochastic optimization technique for constructing analytic continuation

Inversion of Eqn (13) refers to an ill-posed problem [36]. Due to scarcity of information about the values of $G_{\mathbf{k}}(\tau)$ (the function $G_{\mathbf{k}}(\tau)$ is known on a discrete set of imaginary times in the finite range $[0, \tau_{\max}]$), and because of the statistical noise present in the Monte Carlo data, there is, generally speaking, no spectral density $L_{\mathbf{k}}(\omega) > 0$ which would reproduce a given GF $G_{\mathbf{k}}(\tau)$. On the other hand, there exists an infinite set of solutions which do reproduce the GF with a certain amount of deviation, and the problem inevitably arises in respect to which of them to choose. Another, and the most challenging, problem is that the function $L_{\mathbf{k}}(\omega)$ exhibits 'sawtooth' instability when Eqn (13) is solved by any standard approach, for example, by a direct least square minimization of the functional

$$D\big[\widetilde{L}_{\mathbf{k}}(\omega)\big] = \int_0^{\tau_{\max}} \big|G_{\mathbf{k}}(\tau) - \widetilde{G}_{\mathbf{k}}(\tau)\big| G_{\mathbf{k}}^{-1}(\tau)\,\mathrm{d}\tau\,, \tag{33}$$

which is a measure of solution deviation.

Here, $\widetilde{G}_{\mathbf{k}}(\tau)$ is the function obtained by applying the integral operator $\widetilde{G}_{\mathbf{k}}(\tau) = \mathcal{F}\big[\widetilde{L}_{\mathbf{k}}(\omega)\big]$ (13) to the approximate spectral density $\widetilde{L}_{\mathbf{k}}(\omega)$. The sawtooth instability distorts the solution $\widetilde{L}_{\mathbf{k}}(\omega)$ in those regions where the true Lehmann function is smooth: the $\widetilde{L}_{\mathbf{k}}(\omega)$ fluctuations often have a much larger amplitude than the value of the true solution $L_{\mathbf{k}}(\omega)$. The standard ways of suppressing the sawtooth instability rely on using the functional analysis results obtained in the early 1960s [40, 41], based on Phillips [42], and Tikhonov [43] regularization method. This method adds a nonlinear functional to the linear deviation measure (33), the functional which acts to suppress the large derivatives of the approximate solution $\widetilde{L}_{\mathbf{k}}(\omega)$. Further development of the regularization method has led to the maximum entropy (ME) method currently most popular in mathematical physics, which, in addition to its fairly clear regularization strategy, enables one to incorporate *a priori* available information on the solution $L_{\mathbf{k}}(\omega)$.

However, the typical Lehmann function of quasiparticles in a boson field consists of δ-function resonances and a smooth, sharp-boundary incoherent continuum [26, 44], so that the large-derivative-damping regularization method fails to reproduce both the sharp peaks and sharp edges. Furthermore, any concrete realization of the method relies on a prespecified discretization of the space of variable ω,

which is a catastrophically poor approximation for this type of spectral functions (see Ref. [26]). And, finally, using the likelihood function, which is a solution selection tool in the ME method, requires that the statistical data noise in the function $G_{\mathbf{k}}(\tau)$ have a Gaussian distribution — which may prove a poor approximation as well [35].

The recently developed stochastic optimization (SO) [26] method gets around the basic difficulties one encounters in the ME method. The SO idea is first to employ a stochastic procedure to generate a large enough set of M statistically independent, nonregularized particular solutions $\{\widetilde{L}^s_{\mathbf{k}}(\omega)\}, s = 1, ..., M$ whose deviation measures D^s are less than a certain limiting measure D_u determined by the statistical data noise in the function $G_{\mathbf{k}}(\tau)$. Using the linear property of relations (13), (33), the final solution is then determined as the average of

$$L_{\mathbf{k}}(\omega) = M^{-1} \sum_{s=1}^{M} \widetilde{L}^s_{\mathbf{k}}(\omega) \,. \tag{34}$$

The particular solution $\widetilde{L}^s_{\mathbf{k}}(\omega)$ is parameterized as the sum

$$\widetilde{L}^s_{\mathbf{k}}(\omega) = \sum_{t=1}^{K} \chi_{\{P_t\}}(\omega) \tag{35}$$

of rectangles $\{P_t\} = \{h_t, w_t, c_t\}$ with

$$\chi_{\{P_t\}}(\omega) = \begin{cases} h_t \,, & \omega \in \left[c_t - \dfrac{w_t}{2}, c_t + \dfrac{w_t}{2}\right] , \\ 0 \,, & \text{in the opposite case,} \end{cases} \tag{36}$$

defined by continuous parameters such as the height $h_t > 0$, the width $w_t > 0$, and the center c_t. The configuration

$$\mathcal{C} = \left\{\{P_t\},\, t = 1, ..., K\right\} , \tag{37}$$

under the condition

$$\sum_{t=1}^{K} h_t w_t = 1 \,, \tag{38}$$

defines the function $\widetilde{G}_{\mathbf{k}}(\tau)$ in analytic form for any value of τ:

$$\widetilde{G}^{\mathcal{C}}_{\mathbf{k}}(\tau) = \begin{cases} 1 \,, & \tau = 0 \,, \\ 2\tau^{-1} \sum\limits_{t=1}^{K} h_t \exp(-c_t\tau) \sinh\left(\dfrac{w_t\,\tau}{2}\right) , & \tau \neq 0 \,. \end{cases} \tag{39}$$

It should be noted that the specific form of parametrization is of no fundamental importance. What is essential is that the parameters specifying the terms in sum (35) be continuous and that expression (39) have a simple analytical form, which is important for rapidly finding a particular solution. In the procedure for finding a particular solution, a certain initial configuration $\mathcal{C}^{\text{init}}_s$ (37) selected by a random number generator is subjected to a sequence of random changes until solution deviation (33) becomes less than D_u. Because the number of rectangles K is being changed in the course of the optimization, any spectral function can be reproduced to any prespecified precision by a particular solution.

Whereas each particular solution $\widetilde{L}^s_{\mathbf{k}}(\omega)$ contains sawtooth noise in the region of the smooth incoherent continuum, the stochastic nature of the procedure looking for an individual solution does indeed result in that the sawtooth noise in sum (34) is averaged without the suppression of large derivatives. Thus, the smooth portion of the spectrum is not distorted by the sawtooth noise, nor are the sharp peaks and edges smeared due to the absence of regularization smoothing in the SO procedure. Because of the continuous parametrization, any prespecified fragmentation is sure not to occur in a frequency space. Finally, because the final solution is searched as an average of a large number of representative solutions, the Hilbert space of probable solutions is subject to direct sampling, without any assumptions on the form of the likelihood function. Given that such a simple method resolves the traditional difficulties of its classical predecessors, it is puzzling, of course, why it was not developed years ago. The explanation lies in the fact that it is only with the power of modern computers that not just one, as in classical methods, but — as is necessary for implementing the SO method — hundreds and thousands of solutions can now be generated within a reasonable execution time.

Recent successful applications of the SO method have been the reconstruction of the Lehmann functions of Frölich's polaron [26], and the recovery of that for a phonon-coupled hole in the $t-J$ model [32] and of the Rashba – Pekar exciton – polaron [44]. In the last case, the reliable restoration of δ-function peaks inaccessible by regularization methods was especially important because of the presence of several sharp peaks in the Lehmann function. The application of the method to calculating optical conductivity is considered in Ref. [31]. Moreover, the SO method has proved useful not only for the study of excited states but also for the characterization of the ground state in the case when the DMC method fails to provide satisfactory data for the asymptotically large imaginary time in the GF in Eqns (13) – (16). For example, the sign fluctuations in the expansion terms entering Eqn (27) in the problem of a hole in the $t-J$ model prevent calculating the GF for asymptotically large imaginary times, and the GF values can only be obtained for small τ [28]. However, the SO method was capable of providing the energy and Z-factor values even in this case [28]. One recent application of the SO method was to construct analytic continuation in the problem of a phonon-coupled spin system [45].

3. Some aspects of the exciton – polaron problem

This section deals with the major aspects of exciton – polaron physics, which had been understood incompletely or even incorrectly before the recent advent of the DMC and SO methods. In particular, Section 3.2 discusses the polaron self-trapping phenomenon, and Section 3.3 examines the rather old, but still controversial concept of a relaxed excited state (RES). Polaron properties near the end point of the spectrum and the formation conditions of a 3D charge-transfer exciton are covered in detail in Section 3.4 and Section 3.5, respectively. A detailed discussion of angle-resolved photoemission spectra of high-temperature superconductors is given in Section 3.6. Finally, Section 3.7 briefly lists problems where difficulties of a fundamental nature can be readily resolved by using the DMC and SO methods. Section 3.1 which now follows addresses the existing difficulties and related 'blank spots' in the problem of polarons.

3.1 Theoretical challenges

A stumbling block for theoretical methods, the exciton – polaron problem (1) – (4), has as yet evaded exact solution. Moreover, except for certain limiting cases, no analytical

solutions are even available for relatively simpler problems concerning the behavior of an exciton in a rigid lattice [see Eqns (1), (2)] and a single structureless polaron [see Eqns (7)–(9)].

For example, for the exciton problem (1), (2), the only cases to have been solved analytically are the small-radius Frenkel [46] and large-radius Wannier [47] regimes — with no knowledge however, even here, as to the applicability limits of the approximations used. All other known analytical approaches use the random phase approximation (RPA) to solve the equations of motion [21, 22]. Even though these methods can highlight some qualitative features of the intermediate-radius regime, their quantitative value is eliminated by noncontrollable errors introduced by RPA. The most credibility should be given to the numerical approaches that employ the time-dependent density functional theory (see the review [48]) and the solution of the Bethe–Salpeter equation [49–51]. Following the density functional theory, the true four-pole GF is replaced by an effective two-pole one [48], leaving the self-consistent solution of the Bethe–Salpeter equation as the only classical method capable of calculating the two-particle exciton GF (10). However, solving a self-consistent equation implies using a prespecified mesh in momentum or direct coordinate space — a requirement which introduces a systematic error and is a bottleneck of the method. Even today, the numerical solution of the Bethe–Salpeter equation is unable to correctly reproduce the Wannier regime [50]. It follows then that the DMC method, which does not involve the finite discretization of reciprocal space [29], is the only method capable of accurately establishing the usability conditions for the Frenkel and Wannier approximations in a macroscopic system (see Section 3.5).

A similar situation takes place in the simplest case of a structureless polaron, for which analytical solutions are known only in the weak coupling (perturbation theory) and strong coupling (adiabatic approximation) limits. A closer look at the theoretical results obtained for these extremes leads to the conclusion that even in these cases reliable results are available only for the ground state; excited states have so far resisted study, whether treated perturbatively or in the adiabatic approximation. In determining the ground-state parameters of a polaron in the adiabatic approximation, the lattice deformation is assumed to be static and the electronic quantum state is determined variationally. Thus, minimizing the total energy $E(\epsilon) = \langle \psi_G + \epsilon\psi' \mid \widehat{H} \mid \psi_G + \epsilon\psi' \rangle$ yields the wave function ψ_G and the ground-state energy $E(\epsilon \to 0)$. The ground state in the strong coupling approximation can be treated adiabatically because it is much lower in energy than any other state, which differs by just one lattice vibrational quantum. However, neither the variational principle nor the adiabatic approximation are applicable to excited states, especially to those forming a degenerate continuum. Furthermore, the variational approach is even in doubt in the case of a nondegenerate excited level. The energy of an excited state is generally obtained by minimizing the energy for the electron wave function which is taken to be orthogonal to that of the ground state, while otherwise quite arbitrary in form [15]. However, the variation error $\epsilon\psi'$ in the ground-state wave function is proportional to ϵ, compared to the small error $\sim \epsilon^2$ in the energy. Hence, one has absolutely no control over the error in the excited-state wave function being orthogonalized to its ground-state counterpart.

As an example of a long-standing misconception due to unjustifiably applying the variational method to excited states, the concept of a relaxed excited state (RES) will be discussed in Section 3.3. By this concept, which became a subject of close scrutiny [8, 52–55] after its introduction by Pekar [15] many years ago, is meant a quasistable state in which lattice deformation has adapted itself to the excited electronic wave function. However, the DMC and SO calculations of the Lehmann function [26, 56] and optical conductivity [31] showed that in the strong coupling limit RES is not observed due to multiphonon decay processes. It should be noted, finally, that even in the weak coupling limit the perturbation theory may not be applicable to excited states. For example, the perturbation-theory-produced Lehmann function of the Frölich polaron

$$L_{\mathbf{k}=0}(\omega) = \alpha\left[\pi\omega^2(\omega - \omega_{\mathrm{ph}})^{1/2}\right]^{-1}\theta(\omega - \omega_{\mathrm{ph}}) \tag{40}$$

diverges at the phonon energy ω_{ph}, implying that even in this limit an exact method is required [26].

If analytical methods are, with all the above restrictions, applicable to weak and strong coupling regimes, their intermediate coupling results are generally questionable. For example, comparison with the exact result [26] showed that the intermediate coupling theory of Lee, Low, Pines [57] is valid only for weak coupling. On the other hand, it is the intermediate regime found most often in nature, which is of most interest. Adding to this interest is the self-trapping phenomenon specific to this regime, in which, speaking in general terms, a slight change in the parameters of the system causes a strong change in the properties of a particle [9]. For a certain critical value γ_c of the coupling constant, a trapped state residing within a strongly deformed region of the lattice has the same energy as a delocalized state in a weakly deformed lattice. Clearly, the delocalized state is lower in energy in the weak coupling case, but above the critical coupling constant γ_c the relative position of the states is reversed [19, 58]. In other words, a strict quantum-mechanical definition of the self-trapping phenomenon implies the crossing and hybridization of stable (or metastable) polaronic states characterized by very different lattice deformations. On the other hand, a quite general theory exists, thanks to Rashba and Toyozawa, in which rigorous criteria for the occurrence of the self-trapping phenomenon are formulated [19, 58], based on the adiabatic analysis of the system's ground state. In this theory, the self-trapping shows itself if the adiabatic potential of the ground state has a barrier which separates the global minimum from a higher-lying local one. It should be noted that in this adiabatic formulation the complex multiparticle physics of interaction between the ground and excited states is projected on the properties of just one lower sheet of the adiabatic potential, whereas self-trapping is crucially related to excited states. Thus, methods for studying this phenomenon should use no approximations when obtaining results for the excited states.

Among the rather limited number of numerical approaches capable of dealing with excited polaron states may be mentioned the traditional method of exact diagonalization [59–62], well suited for small, usually 1D, lattices (up to 20 sites [60]) with a 'truncated' phonon basis. However, results obtained on finite clusters are only approximate ones as far as a macroscopic system is concerned, and the resulting energy values are not variational in the thermodynamic limit [63]. Special among various versions of the exact diagonalization method is a rather efficient variational method of exact translation [63–67], in which the diagonalization process

employing the variational basis is performed in the sector of the given momentum, thus validating the results in the thermodynamics limit. However, because the basis in the momentum space is determined as a Bloch combination of variational functions in the direct space, the method runs into difficulties when dealing with long-range interactions and with dispersive (especially acoustic) phonons, because of the catastrophic increase of the variational basis. Besides, the method is valid only for small enough values of the adiabatic parameter, $t/\hbar\omega_{\rm ph} \leqslant 5$, and, to add to the problem, has sufficient accuracy only for a few of the lowest discrete states [67]. As a consequence, even for the simplest models with short-range interaction and dispersionless phonons, continuum states are beyond this method. The only approach which permits calculation of incoherent continuum states in some cases is the recently developed cluster perturbation theory, in which exact diagonalization within a cluster is complemented by perturbatively accounting for intercluster transitions [68, 69]. However, the application of this method to the calculation of the spectral function is limited to 1D (or, for some special conditions, 2D) systems with short-range interaction.

Many of the difficulties described in this section are easily overcome by the DMC and SO methods, with which problems (1)–(4) are treated in the most general form and without any approximations. Below, some of the results obtained by these methods are presented.

3.2 Self-trapping

The self-trapping phenomenon, by definition, shows itself as the energy resonance between two polaronic states bound up with different lattice distortions. The first rigorous definition of this phenomenon, which was given within the adiabatic approximation framework, relies on the analysis of the local stability of a delocalized state with zero lattice distortion, $\Delta = 0$, against the energy gain due to a finite distortion $\Delta' \neq 0$. In other words, self-trapping occurs when there is an adiabatic potential barrier between an absolutely delocalized state with $\Delta = 0$ and a trapped state with nonzero deformation $\Delta' \neq 0$. One of these states is stable, while the other metastable. The criterion for the existence of the potential barrier is determined by the stability index

$$s = d - 2(1 + l)\,, \tag{41}$$

where d is the dimension of the system. The l index stands for the degree of force range: $\lim_{q\to 0}\psi(q) \sim q^{-l}$, where $\psi(\mathbf{R})$, the kernel of the interaction $U(\mathbf{R}_n) = \psi(\mathbf{R}_n - \mathbf{R}_{n'})\, v(\mathbf{R}_{n'})$, relates the potential $U(\mathbf{R}_n)$ acting on the particle to the generalized lattice distortion $v(\mathbf{R}_{n'})$ [19]. The barrier exists if $s > 0$ and does not exist if the inequality goes the other way. Hence, according to adiabatic theory, two states with different Δ can coexist for $s > 0$. The ground-state lattice deformation undergoes a sudden change at the critical value of the coupling constant, when the energy levels cross. However, the first-order (in the coupling constant) transition is an artefact of the adiabatic theory because the nonzero matrix element of a nonadiabatic interaction actually causes hybridizative mixing of these states. Thus, the self-trapping phenomenon is a crossover rather than a sharp transition, and all properties of the polaron are analytical with respect to the coupling constant (for a rigorous proof, see Ref. [70]). This analyticity makes the definition of self-trapping rather vague because trapped and delocalized states always mix with one another. For example, we cannot even claim a separate class for a boundary case in the adiabatic theory at $s = 0$, where two states never coexist, but a sharp transition between them does occur at a certain critical point. Furthermore, even in the case $s < 0$, for which adiabatic theory rules out the existence of a potential barrier, states with different lattice deformations can still resonate with one another. Criterion (41) only rejects the coexistence of $\Delta = 0$ and $\Delta' \neq 0$ states, not of two different states with nonzero deformations ($\Delta' \neq \Delta$). Finally, the separation of states into trapped ones and delocalized ones may not be valid in a strict sense because at the self-trapping point more than two states can mix, provided they all fall within the energy scale of the nonadiabatic matrix element.

However, even though adiabatic theory lacks rigor in defining self-trapping phenomenon, it provides considerable insight into the process. In the weak coupling limit, the lowest state is bound up with a weakly deformed lattice, whereas the upper state(s) are coupled strongly to the lattice. On the other hand, in the strong coupling regime, when the states have already interacted and exchanged with one another at the critical coupling constant $\gamma_{\rm c}$, the opposite situation prevails for the properties of these states, with the lowest state trapped and the upper state(s) delocalized. However, simple as this intuitive picture is, it has not yet been explicitly demonstrated. Extensive numerical work on the subject (see the book [19] and references cited therein) is mostly concerned with ground state properties, and results on excited resonances are always compromised by uncontrollable approximations.

The first explicit, approximation-free demonstration of the above intuitive picture was put on by the DMC and SO methods in Ref. [44], which studied dependence on the coupling constant of the physical properties of the ground and excited states of a 3D Rashba–Pekar exciton–polaron [71, 72], a system with a short-range ($l = 0$) couple to dispersionless phonons ($\omega_{\rm ph} = 1$). In this case, the stability index is $s = 1$, enabling one to observe the classical features of the adiabatic self-trapping scenario. The ground state properties calculated in Ref. [44] are fully consistent with the adiabatic picture. In the neighborhood of the critical coupling constant, the average number of phonons $\langle N \rangle$ in the polaron cloud shows a sudden, orders-of-magnitude change, as does the effective mass. Furthermore, Ref. [44] demonstrated the nature of the quantum resonance between two states. The distribution (18) over phonons in the polaron cloud, $Z^{(\mathbf{k}=0)}(n)$, has a maximum at $n = 0$ in the weak coupling regime (which corresponds to a weak lattice deformation), and a maximum for $n \gg 1$ under strong coupling (significant lattice deformation). Near criticality, however, two very distinct peaks — at $n = 0$ and for $n \gg 1$ — are found, which can be interpreted as a quantum mixture of states with very different deformations.

In the vicinity of the critical point ($\gamma_{\rm c} \approx 18$), the polaron Lehmann function has several stable states (Fig. 2) below the energy threshold of the incoherent continuum, $E_{\rm g.s.} + \omega_{\rm ph}$, above which excitation is unstable due to transitions to the ground state (with energy $E_{\rm g.s.}$) with the emission of a phonon of energy $\omega_{\rm ph} = 1$. The way the energies of the ground state and stable excited states depend on the coupling constant is akin to the crossing pattern of a number of interacting levels, being consistent with what adiabatic theory predicts (Fig. 3). The only — but very important — qualitative difference resides in that not two but at least three states are involved in the hybridization process. The most important result of

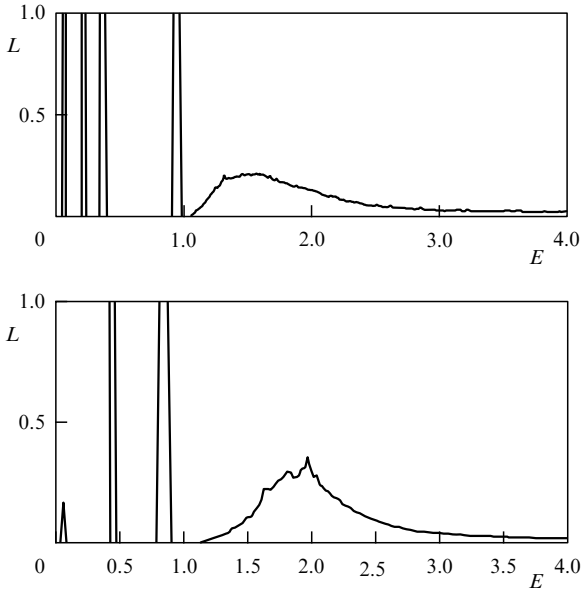

Figure 2. Lehmann function $L_{(\mathbf{k}=0)}(E)$ for critical coupling $\gamma = \gamma_c$ (top), and for $\gamma > \gamma_c$ (bottom). Energy is measured from the polaron ground-state level $E_{g.s.}$.

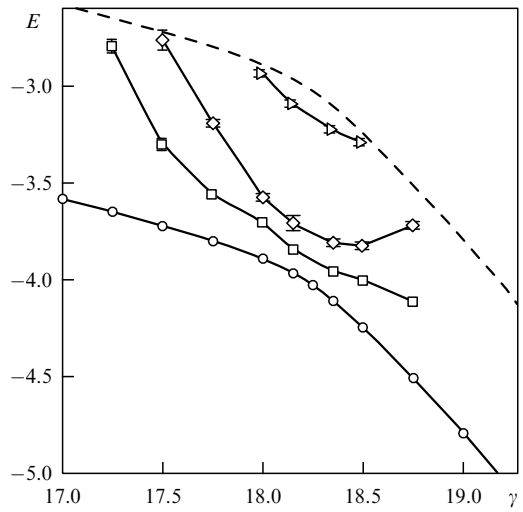

Figure 3. Coupling constant dependence of the ground state (open circles) and stable states (squares, diamonds, and triangles). Dashed line depicts the incoherent continuum threshold.

Ref. [44] is a direct demonstration of the fact that below critical coupling constant an excited state is one with a large effective mass. In accordance with the adiabatic picture, in the weak coupling regime the lowest state with zero momentum has a small effective mass m^* on the order of the bare mass m, while the effective mass of an excited trapped state is large, $m^* \gg m$. It follows then that the ground state with low effective mass will, at a certain momentum, reach the energy of the flat band of the excited state. Following this, increasing the momentum makes these states interchange. Figure 4 demonstrates the change in the ground state properties with increasing momentum: at the intersection of the flat branch of the excited state, the average number of phonons in a polaron cloud sharply increases, and the dispersion becomes flat.

Above the self-trapping point the situation is reversed, i.e., the ground state has a large effective mass, and an excited

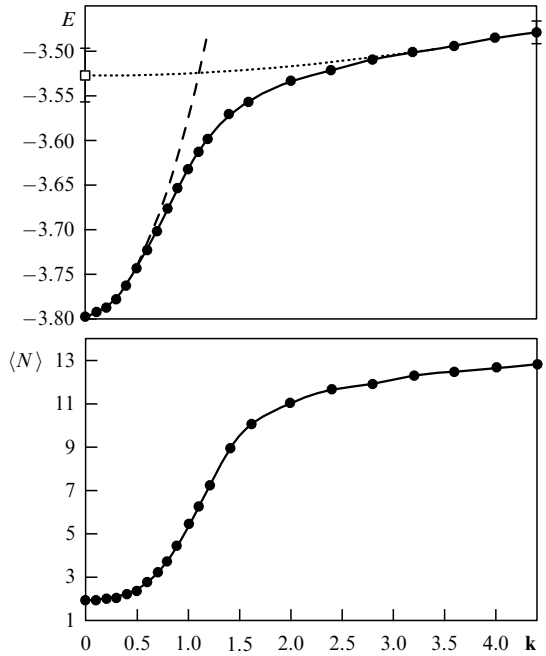

Figure 4. Wave vector dependence of energy (top) and average number of phonons (bottom) in a polaron cloud for $\gamma < \gamma_c$ (full circles connected by solid lines). The dashed line displays the effective mass approximation $E^{(\mathbf{k})} = E_{g.s.} + \mathbf{k}^2/2m^*$ for $E_{g.s.} = -3.7946$ and $m^* = 2.258$. These values were obtained by the DMC method for the given coupling constant γ. The dotted line portrays the parabolic law fitted to the last four points of the curve with parameters $E_1 = -3.5273$ and $m_1^* = 195$. The open square is the energy of the first excited state at zero momentum, as derived from the spectral analysis for the given coupling constant.

state a small one. The special features of this case are described in the work [32] on the self-trapping of a hole in a 2D $t-J$ model with strong short-range interaction with dispersionless optical phonons (see Section 3.6 for more details). It should be noted that although the stability index of this system is not positive, $s = 0$, the model most clearly demonstrated all those features of the self-trapping crossover, which were predicted in the adiabatic approximation. However, the hole in the $t-J$ model interacts not only with optical phonons but also with acoustic magnons, thus invalidating the necessary conditions of criterion (41).

The self-trapping phenomenon has also been observed in a 1D system [27, 73] with quasidegenerate states (4) – (6) and a short-range interaction ($l = 0$). In a 1D system, the stability index s is always smaller than zero, making self-trapping impossible in view of criterion (41). The results of Refs [27, 73], however, are not at odds with criterion (41) because this criterion was obtained for a single nondegenerate state. Besides, it takes special conditions for states with different lattice deformations to resonate in the model constructed in Refs [27, 73]. A sharp transition with respect to the coupling constant $\gamma_{i \neq j}$ of the nondiagonal interaction (6) occurs only in the presence of a strong diagonal interaction at one of the levels. This self-trapping mechanism directly follows from the balance of diagonal and nondiagonal interactions operative in a quasidegenerate system and, based on the qualitative analysis in Ref. [74], can be realized in a molecular system as well.

Self-trapping has not been observed for the 3D Frölich polaron interacting with dispersionless optical phonons [26, 56]. In this case, all physical properties of the ground state

were smooth with respect to the coupling constant, and no additional resonances were found below the energy $E_{\text{g.s.}} + \omega_{\text{ph}}$ of the incoherent continuum. This result agrees with the adiabatic theory, however, because for a system with long-range polarization interaction ($l = 1$) the stability index is less than zero: $s = -1$.

In conclusion, DMC and SO results on self-trapping have for the first time revealed the key features of this phenomenon without utilizing any approximations. It was shown that this phenomenon is related to the quantum resonance between states with different lattice deformations, one of them being coupled weakly, and the other strongly, to the lattice. Exact numerical methods have shown that while stability index (41) is adequate for describing the properties of a structureless polaron, it must be used with caution whenever a complication is introduced into the problem.

3.3 The relaxed excited state concept

Prior to the advent of the exact DMC and SO methods [31], the optical conductivity (OC) $\sigma(\omega)$ of the Frölich polaron was the subject of heated theoretical controversy, even in the strong coupling regime. The adiabatic variational treatment of the strongly coupled polaron [15] predicts the so-called relaxed excited state (RES), namely, a quasistable state in which the lattice has adapted itself to the electronic wave function of an excited state. For this state to show up as a sharp peak in the OC spectra, its decay rate must be sufficiently small — otherwise the very concept of a quasistable state becomes meaningless. In Ref. [53], a one-phonon approximation estimate for the RES decay rate was obtained, on the basis of which the OC spectrum was predicted to have a sharp peak in the strong coupling regime — a prediction which was confirmed in Ref. [54] by expanding the impedance $Z(\omega)$ within the Feynman – Hellwarth – Iddings – Platzman (FHIP) [75] approach. The validity of the one-phonon approximation [53] in the strong coupling regime is quite doubtful, however, and expanding the inverse impedance $1/Z(\omega)$ in the same FHIP framework [75] revealed no sharp peak in OC. A check therefore had to be carried out on whether or not the RES is an artefact of the impedance-expansion-based method of calculating the optical conductivity $\sigma(\omega)$:

$$\sigma(\omega) \sim \left(Z_0(\omega) + Z_1(\omega) + \dots\right)^{-1}, \tag{42}$$

because in this approach even the lowest-order approximations show a resonance structure in OC.

An exact computation of the Lehmann function of the Frölich polaron in Ref. [26] threw into doubt the concept of the RES. As predicted by the adiabatic theory [55], in the strong coupling limit the RES energy relative to the polaron ground state is proportional to the square of the dimensionless coupling constant of the polarization interaction, $\alpha \sim \gamma$. However, no such peak has been observed in the strong coupling regime [26]. Instead, rather broad peaks have been examined against the incoherent background, whose energies depended weakly on α (Fig. 5). An exact calculation [31] did not reveal the presence of RESs in OC spectra in the strong coupling regime, either. The applicability of the RES concept was investigated by comparing the exact DMC and SO optical conductivity spectra with the approximate predictions of Ref. [54] based on impedance expansion (42). In the approximate solution, RES appears for $\alpha \geqslant 5$ as a broad peak, which gets narrower as the coupling constant is

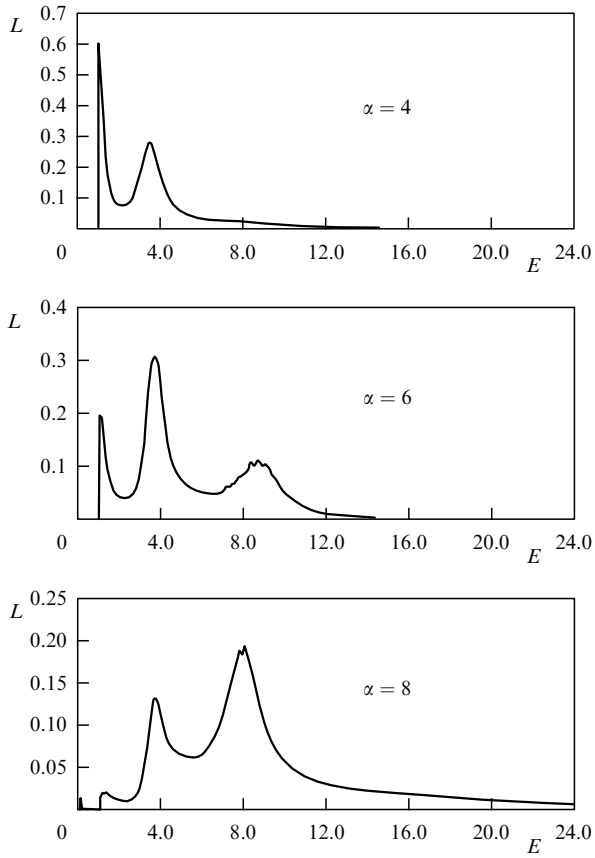

Figure 5. Evolution of spectral density as a function of α in the transition region from intermediate to strong coupling. The polaron ground-state peak is shown only for $\alpha = 8$ because at smaller coupling constants it highly exceeds the vertical scale used. Energy is measured from the polaron ground state.

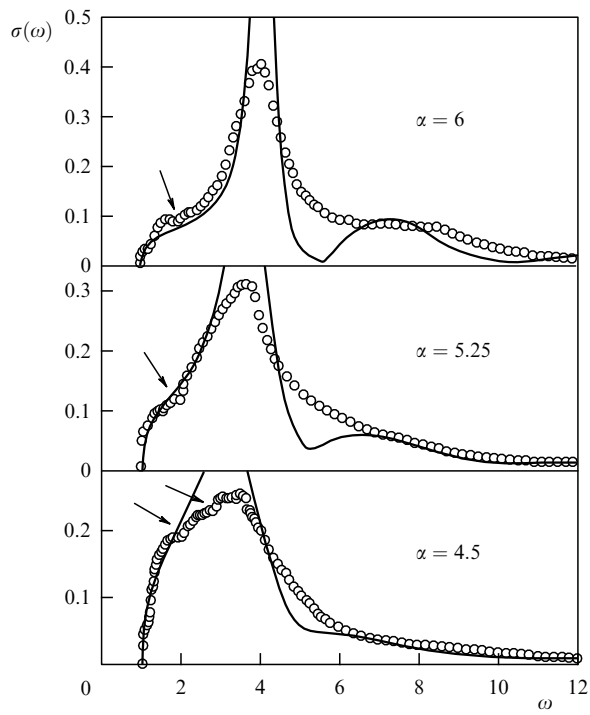

Figure 6. Optical conductivity in the intermediate coupling regime (open circles) as compared with the results of Ref. [54] (solid line). Arrows indicate absorption spectrum anomalies arising on two- and three-phonon thresholds.

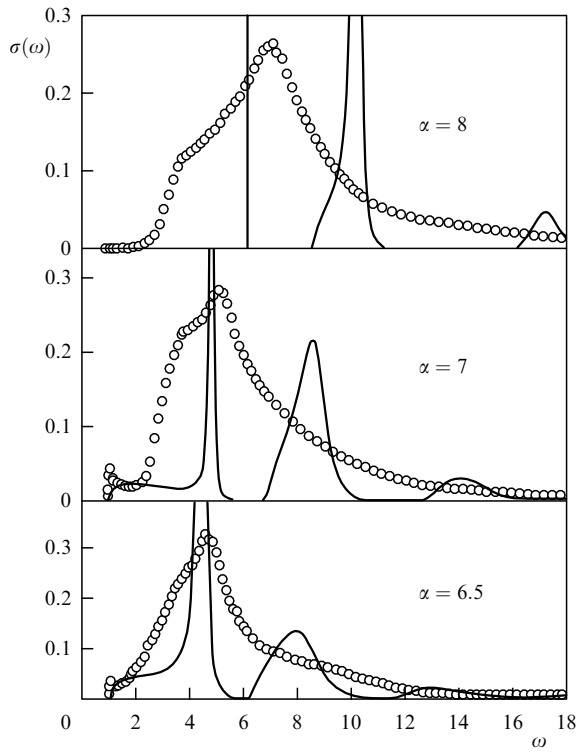

Figure 7. Optical conductivity in the strong coupling regime (open circles) as compared with the results of Ref. [54] (solid lines).

increased further. The exact OC computation supports the appearance of a broad peak for $\alpha \geqslant 5$ at exactly the energy values predicted in Ref. [54]. Moreover, the peak starts narrowing as the coupling constant is increased within the range $5 < \alpha < 6$ (Fig. 6). As the coupling strength increases further, however, the optical conductivity peak starts to become much broader instead of narrower (Fig. 7). It should be stressed that the peak broadening obtained with the DMC and SO techniques is not an artefact of the numerical analytic continuation because even such fine details as two- and three-phonon absorption thresholds are resolved in the OC spectra (see Fig. 6). It can therefore be concluded that, for all its physical appeal and despite its arising so naturally from the variational approach in the strong coupling limit, the concept of RES cannot be employed in interpreting the optical spectra of the Frölich polarons, especially in the case of strong electron – phonon interaction.

3.4 The end point of the polaron spectrum

The end point of the polaron spectrum refers to the momentum k_c for which the stable ground state of the polaron vanishes. This occurs when the energy of the polaron becomes greater than the threshold energy for the emission of a real phonon — that is, greater than the energy of an optical phonon. In accordance with the general theory [33, 76], in the vicinity of the end point of its spectrum a polaron can be considered as a weakly bound state of a phonon which carries all the momentum of the state, and an electron with near-zero momentum.

This easy-to-understand physics was illustrated in Refs [25, 26] by calculating the dispersion and structure of the Frölich polaron's phonon cloud for momentum $\mathbf{k}'$ of absolute magnitude slightly less than that of the limit point k_c. The computations showed that the partial weight distribution of n-phonon states $Z^{(\mathbf{k}')}(n)$, determined by Eqn (18), has a sharp peak at $n = 1$ and that the very distinct peak of the one-phonon distribution function

$$F(\mathbf{q}) = \sum_{n=1}^{\infty} n^{-1} \sum_{j=1}^{n} \sum_{\mathbf{q}_1, \ldots, \mathbf{q}_{j-1}, \mathbf{q}_{j+1}, \ldots, \mathbf{q}_n} |\theta(\mathbf{k}'; \mathbf{q}_1, \ldots, \mathbf{q}_j = \mathbf{q}, \ldots, \mathbf{q}_n)|^2 \tag{43}$$

coincides with the polaron momentum.

3.5 The exciton

The applicability limits of the Wannier and Frenkel exciton models were investigated in Ref. [29] using the DMC method. The one-particle electron – hole spectrum of the 3D system was taken to consist of a conduction band and a valence band, both of width E_c and both symmetric, which are separated by a zero-momentum gap of width E_g. For large (more than 30) values of the ratio $W = E_c/E_g$, the exciton binding energy (21) for zero momentum ($\mathbf{k} = 0$) agrees well with the results for the Wannier limit (Fig. 8), and the probability density $|\xi_{\mathbf{k}=0,\mathbf{p}}(\text{g.s.})|^2$ for the wave function of the relative electron – hole motion corresponds to the hydrogen-like case (Fig. 9a). The unexpected result is that the valence and conduction bands must be very wide ($W > 20$) for the Wannier approximation to be adequate. For lower values of W, both the binding energy E (Fig. 8) and the wave function of relative motion (Fig. 9b) differ considerably from their large-radius approximation results. Furthermore — and this is the most interesting result of the validity analysis of the small-radius approximation — it turned out that a strongly trapped wave function does not at all ensure that the Frenkel model correctly accounts for the energy of the exciton. For $1 < W < 10$, even though the wave function already has a dominant single-site component, the exciton binding energy differs radically from what the Frenkel model predicts it to be. In addition, for $E_c/E_g = 0.4$, when the wave function is already almost completely trapped (Fig. 9c), the binding energy is half of its small-radius approximation value (see

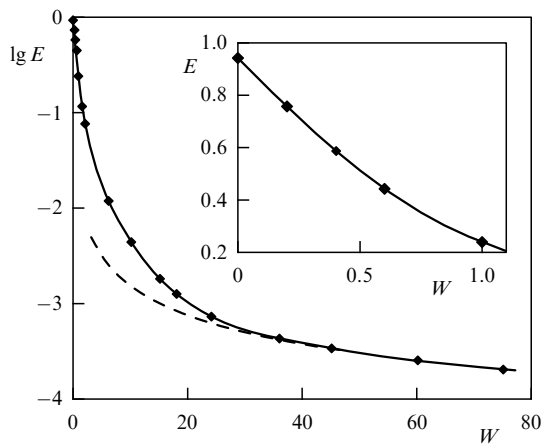

Figure 8. Exciton binding energy versus the relative width $W = E_c/E_g$ of the valence and conduction bands. The dashed line is the Wannier approximation; the solid line depicts the cubic spline with derivatives determined by the Wannier limit and perturbation theory at the right and left ends, respectively. The inset shows the initial portion of the plot.

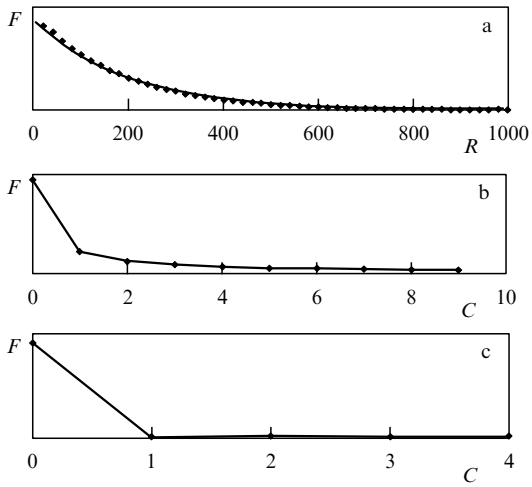

Figure 9. Wave function of internal motion in a direct space: (a) Wannier regime ($W = 60$); (b) intermediate radius regime ($W = 10$), and (c) Frenkel regime ($W = 0.4$). The wave function in the Wannier regime is spherically symmetric, whereas in the intermediate and Frenkel regimes it is governed by the lattice, which makes the number C of the coordination sphere the natural choice for the abscissa in two last regimes. The solid line in figure (a) represents the Wannier model result and serves to join data points elsewhere.

inset to Fig. 8). The deviation of the binding energy E from the Frenkel approximation result E_{F} is well described by the empirical formula $E \approx E_{\mathrm{F}} - W$ in a wide range of $W < 0.4$, implying that this deviation is determined by the kinetic energies of electron and hole delocalization. And finally, the conclusion can be drawn that in practically most cases the Frenkel and Wannier approximations are quite restricted in their applicability.

As regards another major result, the authors of Ref. [29] calculated conditions for the formation of a charge-transfer exciton in a 3D system — something which has long been a subject of discussion in the field of compounds with unstable valence [77]. In Refs [78, 79], the unusual properties of fluctuating valence compounds were explained by the excitonic instability of the optically forbidden monopole charge-transfer exciton. Although the excitonic instability model has provided a quantitative explanation for phonon spectra [80, 81], optical properties [82, 83], and peculiarities in neutron magnetic scattering [84], its underlying charge-transfer exciton idea came under severe criticism in Ref. [85]. To investigate the exciton structure in fluctuating valence compounds, the conduction and valence band dispersions were taken in the form typical for these materials, namely, as a nearly flat valence band separated by an indirect gap from a broad conduction band with a maximum at zero momentum and a minimum at the Brillouin zone boundary. A computation [29] for such a band structure confirmed that the monopole exciton is indeed related to charge transfer because its was found that the wave function of internal motion has almost a zero single-site component and a charge density maximum at the nearest-neighbor sites.

3.6 A phonon-coupled hole in the $t-J$ model

The special interest in the mysterious properties of high-temperature superconductors have drawn attention to the thorough study of the problem of a single hole in a Mott insulator. The literature abounds in studies concerning the limiting case of the strong Hubbard repulsion, i.e., the so-called $t-J$ model [4] with

$$\widehat{H}_{t-J} = -t \sum_{\langle ij \rangle s} c_{is}^{\dagger} c_{js} + J \sum_{\langle ij \rangle} \left(\mathbf{S}_i \mathbf{S}_j - \frac{n_i n_j}{4} \right). \tag{44}$$

Here, c_{js} is a fermion annihilation operator (projected so as to eliminate double occupation), $n_i < 2$ is the occupation number, $\mathbf{S}_i$ is the spin-1/2 operator, J is the exchange integral, and $\langle ij \rangle$ defines the nearest neighbors in a 2D lattice. A variety of theoretical approaches have been developed and used (see reviews [4, 86] and recent studies in Refs [28, 87]) to reveal the major properties of the Lehmann function. In the low-energy part of the spectrum, the hole Lehmann function has a peak, sharp for all momenta and dispersive with a band width $W_{J/t} \sim J$. The more sophisticated $t - t' - t'' - J$ model includes more distant neighbor hopping, thereby changing the dispersion of the quasiparticle resonance [88–94]. However, the quasiparticle peak remains sharp and well-defined for all momenta [96], provided the appropriate model parameters are taken for real, weakly doped high-temperature superconductors under study [89, 95].

Despite this coherent theoretical picture, however, the angle-resolved photoemission spectroscopy (ARPES), a technique capable of measuring the hole Lehmann function [93–95], revealed many mysterious contradictions. On the one hand, the experimentally examined dispersion of the lower peak of the Lehmann function is well described by the $t - t' - t'' - J$ model [88–94]. On the other hand, in clear contradiction to theory, the sharp quasiparticle resonance is never seen in experiments, and instead a broad peak is observed, whose width, 0.1–0.5 eV ($\approx t$), often exceeds the band width. It should be noted that this width has nothing to do with sample imperfections because doping introduces more disorder, and the line width, on the contrary, decreases.

In recent years, numerous experimental data have stimulated renewed interest in electron–phonon interaction effects occurring in high-temperature superconductors. Among the high-impact experimental findings are spectral line broadening and phonon-energy renormalization [100], both explained in terms of interaction with holes [97–99], and the effect of isotopic substitution on the superconducting transition temperature in weakly doped cuprates and on superfluid density in optimally doped materials [101]. Particularly convincing were the experiments that demonstrated the effect of isotopic substitution on optical conductivity spectra [102] and angle-resolved photoemission [103].

The authors of Ref. [32] applied the DMC method to studying the hole Lehmann function in the $t-J$ model in all coupling regimes with dispersionless phonons of frequency Ω. Previous to the work cited, this problem had been treated only in the noncrossing approximation (NCA) [105]. However, in the case of the electron–phonon interaction this approximation is inadequate either for a strong or for an intermediate coupling regime. Reference [32] demonstrated this fact for the Holstein polaron model by using the DMC method which allows the diagrams to be summed exactly both in and without the NCA approximation. Exact and NCA results for energy and the Z-factor agree well at small values of the dimensionless coupling constant $g = \gamma^2/(8t\Omega)$, $g \leqslant 0.2$, but show qualitative differences at large values. For example, at $\Omega/t = 0.1$ the exact result undergoes crossover into the strong

coupling regime for $g > g_{\mathrm{H}}^{\mathrm{c}} \approx 0.6$, whereas with the NCA result this crossover does not occur even at $g = 60$. This means that allowing for the mutual crossing of phonon propagators is crucial for correctly treating the strong coupling regime.

In the standard spin-wave approximation for the $t-J$ model [3, 104], a dispersionless hole $\varepsilon_0 = \text{const}$ travels in the bath of magnons and is scattered by them. The magnon dispersion $\omega_{\mathbf{k}}$ and the interaction vertex $M_{\mathbf{k},\mathbf{q}}$ are taken in standard form [86, 104], whereas the value of the exchange constant $J = 0.3t$ is dictated by the experimental data. If coupled to dispersionless phonons (with experimental frequency $\Omega = 0.1t$), the hole is also scattered by the lattice vibrations, reducing the problem to one of a polaron interacting with several bosonic fields [see Eqns (3), (4)]. A Feynman expansion using the DMC method takes into account the mutual crossing of phonon propagators, while neglecting, due to the sign problem, the crossing of their magnon counterparts. NCA approximation does apply to a hole interacting with a magnetic system because spin $S = 1/2$ cannot flip more than once and because the number of magnons around the hole cannot increase beyond the saturation value. On the other hand, the mutual crossing of phonon diagrams contributes importantly, as is shown by the example of the Holstein polaron.

Figure 10 presents Lehmann functions for the ground-state momentum $\mathbf{k} = (\pi/2, \pi/2)$ in the regimes of weak, intermediate, and strong coupling to phonons. The way in which the peak energies (Fig. 11a) and the ground-state factor $Z^{\mathbf{k}=(\pi/2,\pi/2)}$ (Fig. 11c) vary with the coupling constant is very much akin to what is happening in the self-trapping phenomenon [44, 58]. States cross and hybridize at coupling constants in a narrow range close to the critical value $g_{t-J}^{\mathrm{c}} \approx 0.19$, and the ground-state resonance factor $Z^{\mathbf{k}=(\pi/2,\pi/2)}$ decreases rapidly in this range. The point to note here is that the NCA result is quite different from that when the phonon–phonon vertex part is fully taken into account (Figs 11b and 11c). According to the general picture of self-trapping phenomenon, it is expected that above the critical coupling, $g > g_{t-J}^{\mathrm{c}}$, the lowest state will be dispersionless, and that the excited state will possess a low effective mass. That this is indeed the case is demonstrated in Fig. 12, where the momentum dependence of the Lehmann function well above the critical coupling is portrayed. What is surprising is that the upper broad resonance has exactly the dispersion of the pure $t-J$ model (Fig. 13). The momentum

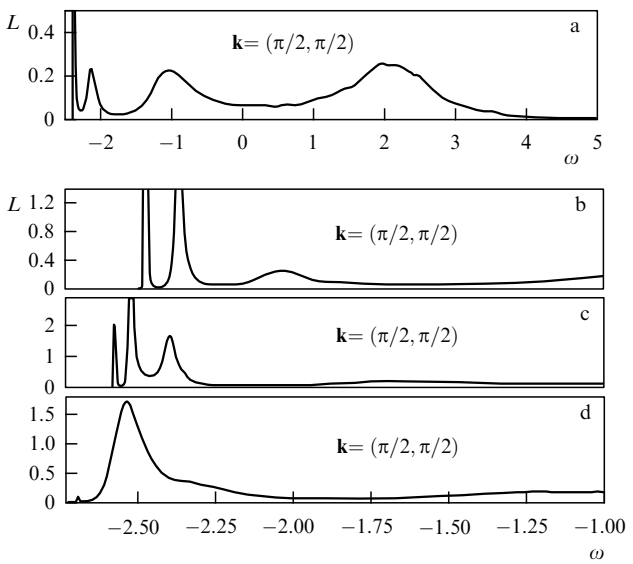

Figure 10. Hole Lehmann function for $\mathbf{k} = (\pi/2, \pi/2)$: (a) $g = 0$; (b–d) low-energy parts: (b) $g = 0.1445$, $\gamma = 0.34$; (c) $g = 0.2$, $\gamma = 0.4$, and (d) $g = 0.231125$, $\gamma = 0.43$.

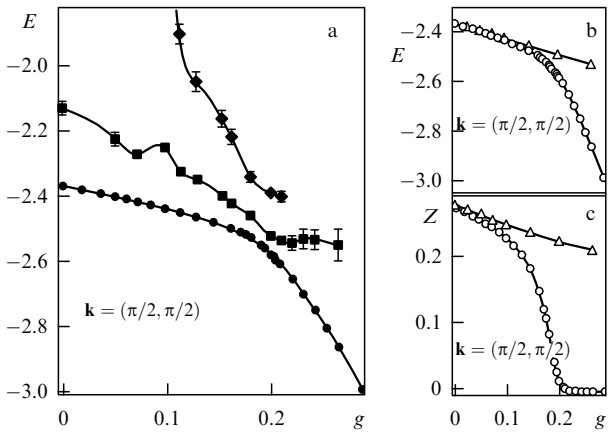

Figure 11. Variation with coupling constant of (a) the lowest resonance energies of the Lehmann function; (b) the energy, and (c) the $Z^{\mathbf{k}=(\pi/2,\pi/2)}$-factor of the lower peak in the exact DMC (open circles) and DMC-NCA (triangles) calculations.

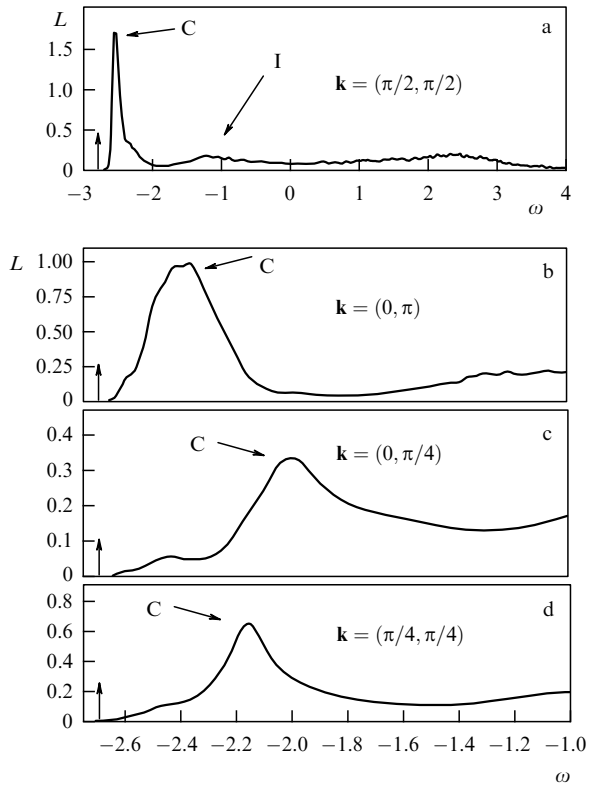

Figure 12. Hole Lehmann function at $g = 0.231125$: (a) the entire energy range at $\mathbf{k} = (\pi/2, \pi/2)$; (b — d) the low-energy part at various momenta. Slanted arrows indicate broad peaks which are interpreted as coherent (C) and incoherent (I) parts in ARPE spectra. Vertical arrows indicate the position of a true quasiparticle, namely, a dispersionless ground-state resonance which is invisible at the vertical scale shown.

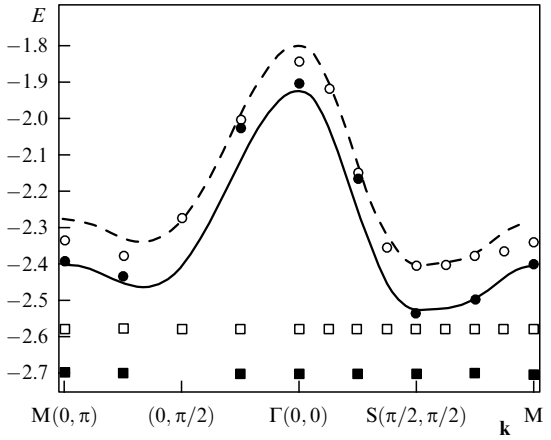

Figure 13. Resonance energy dispersion at $J/t = 0.3$. Circles (the broad resonance) and squares (the lower polaron resonance) are shown full for $g = 0.231125$, and open for $g = 0.2$. The lines are plotted using the dispersion relation (45) for a hole in a pure $t - J$ model at $J/t = 0.3$ ($W_{J/t=0,3} = 0.6$), with $\varepsilon_{\min} = -2.396$ ($\varepsilon_{\min} = -2.52$) shown by a dashed (solid) line.

dependence is given by the relationship

$$\varepsilon_{\mathbf{k}} = \varepsilon_{\min} + W_{J/t}\left\{\frac{\left[\cos k_x + \cos k_y\right]^2}{5} + \frac{\left[\cos(k_x + k_y) + \cos(k_x - k_y)\right]^2}{4}\right\}, \qquad (45)$$

which describes the dispersion of a pure $t-J$ model over a wide range of exchange constants [106]. This property is general for the strong coupling regime (see Fig. 13).

The strong coupling behavior of the Lehmann function is identical to what is observed in the ARPE spectra of undoped superconductors. First, the Lehmann function consists of a broad peak and a high-energy incoherent continuum (see Fig. 12). Second, the dispersion of the broad peak reproduces that of the sharp resonance in the pure $t-J$ model (see Fig. 13). The lowest dispersionless peak has a low weight in the strong coupling approximation and is not observed in experiments. On the other hand, in accordance with experiment, the momentum dependence of the spectral weight $Z^{(\mathbf{k})'}$ of the broad resonance exactly reproduces the dispersion of the $Z^{(\mathbf{k})}$-factor of the narrow resonance in the pure $t-J$ model. The reason is that when the phonon frequency Ω is less than the exchange coupling constant J, then under strong coupling conditions the entire weight of the sharp resonance in the $t-J$ model goes over to a broad dispersive peak.

The explanation in Ref. [32] of the ARPE spectra of weakly doped superconductors unambiguously suggests that the chemical potential has no relation to the broad dispersive resonances observed in these spectra and is instead pinned to an invisible small-Z quasiparticle pole. In a semiconductor, the position of the chemical potential is poorly defined and depends on pinning by defect states. However, even for a small finite doping its position is determined by the valence band top. Despite the obvious nature of this statement, however, the chemical potential in a weak doping regime is quite away from the band top of the resonance observed in the ARPE spectra [107]. This contradiction, according to the results of Refs [32, 107], is due to the fact that the broad ARPES resonance observed in weakly doped superconductors is not a quasiparticle but a set of Franck – Condon phonon excitations.

Comparison of two critical coupling values — one, $g^{\mathrm{c}}_{t-J} \approx 0.19$, for a hole in the $t-J$ model to make the transition to the strong coupling regime, and the other, $g^{\mathrm{c}}_{\mathrm{H}} \approx 0.6$, for the Holstein model with the same parameter values — leads to the conclusion that interaction with spins speeds up the transition of a hole to the self-trapped state. This is due to the fact that the magnons (which are emitted each time the hole makes a hop) narrow the coherent band by the factor J/t, whereas the effective hole – phonon coupling constant is not renormalized by the small $Z^{(\mathbf{k})}$-factor of the $t-J$ model [99]. The point to note here is that the transition to strong coupling regime in the $t-J$ model occurs at such small coupling constants that a hole can be self-trapped in an undoped cuprate. For example, the coupling strength estimated from the energy renormalization and spectral line broadening of the phonons is found to be above the critical coupling for the transition to the self-trapped state.

3.7 Where next?

Because the DMC method is easily extended [30] to the general exciton – polaron problem (1) – (4), it is the exciton – polaron which is a natural candidate for further study. Depending on how strongly the hole and the electron interact with phonons, a host of striking effects can be obtained, for whose study none of the conventional methods is suitable [19]. The influence of the scattering potential of an impurity on these processes can also be treated by the DMC and SO methods because including impurity scattering reduces to trivially adding the scattering potential vertices to the exciton – polaron GF expansion [34].

The DMC method has recently been generalized to the problem of a bipolaron with a single-site Coulomb repulsion and a short-range Holstein electron – phonon interaction [108]. When expanding a GF in momentum space one faces the problem of sign, due to repulsion, but the authors of Ref. [108] overcame this problem in an elegant way by transferring to direct space, where repulsion is diagonal and the sign problem therefore does not arise. This approach can also be adapted to the case where the repulsion and electron – phonon interaction potentials are longer in range.

There is, finally, a large list of acoustic polaron problems, dating back more than forty years [109], which, unless approximated, cannot be solved by any traditional methods and are therefore natural subjects for the application of the DMC technique.

Acknowledgments. The author wishes to acknowledge fruitful discussions with Prof. N Nagaosa. The work was supported by the RFBR grant No. 04-02-17363a.

References

1. Appel J, in *Solid State Physics* Vol. 21 (Eds H Ehrenreich, F Seitz, D Turnbull) (New York: Academic Press, 1968)
2. Firsov Yu A *Polyarony* (Polarons) (Moscow: Nauka, 1975)
3. Kane C L, Lee P A, Read N *Phys. Rev. B* **39** 6880 (1989)
4. Izyumov Yu A *Usp. Fiz. Nauk* **167** 465 (1997) [*Phys. Usp.* **40** 445 (1997)]
5. Ansel'm A I, Firsov Yu A *Zh. Eksp. Teor. Fiz.* **28** 151 (1955); **30** 719 (1956) [*Sov. Phys. JETP* **1** 139 (1955); **3** 564 (1956)]; Toyozawa Y *Prog. Theor. Phys.* **20** 53 (1958)
6. Davydov A S *Teoriya Tverdogo Tela* (Solid State Theory) (Moscow: Nauka, 1976)

7. Toyozawa Y *Optical Processes in Solids* (Cambridge: Cambridge Univ. Press, 2003)
8. Devreese J T, in *Encyclopedia of Applied Physics* Vol. 14 (Ed. G L Trigg) (New York: VCH Publ., 1996) p. 383
9. Landau L *Phys. Z. Sowjetunion* **3** 664 (1933)
10. Fröhlich H, Pelzer H, Zienau S *Philos. Mag.* **41** 221 (1950)
11. Kanamori J *Appl. Phys.* (*Suppl.*) **31** S14 (1960); Abragam A, Bleaney B *Electron Paramagnetic Resonance of Transition Ions* (Oxford: Clarendon Press, 1970); Kugel' K I, Khomskii D I *Usp. Fiz. Nauk* **136** 621 (1982) [*Sov. Phys. Usp.* **25** 231 (1982)]
12. Davydov A S *Teoriya Pogloshcheniya Sveta v Molekulyarnykh Kristallakh* (Theory of Light Absorption in Molecular Crystals) (Kiev: Izd. AN USSR, 1951) [Translated into English: *Theory of Molecular Excitons* (New York: McGraw-Hill, 1962)]; Ray E G *Austr. J. Chem.* **16** 315 (1963)
13. Rashba E I *Zh. Eksp. Teor. Fiz.* **50** 1064 (1966); **54** 542 (1968) [*Sov. Phys. JETP* **23** 708 (1966); **27** 292 (1968)]
14. Bersuker I B, Polinger V Z *Vibronnye Vzaimodeistviya v Molekulakh i Kristallakh* (Vibronic Interactions in Molecules and Crystals) (Moscow: Nauka, 1983) [Translated into English (Berlin: Springer-Verlag, 1989)]
15. Pekar S I *Issledovaniya po Elektronnoi Teorii Kristallov* (Investigations in the Electron Theory of Crystals) (Moscow: Gostekhizdat, 1951)
16. Schultz T D, in *Polarons and Excitons* (Eds C G Kuper, G D Whitfield) (Edinburgh: Oliver and Boyd, 1963) p. 71
17. Vinnitskii V L *Zh. Eksp. Teor. Fiz.* **40** 1459 (1961) [*Sov. Phys. JETP* **13** 1023 (1961)]; Anderson P W *Phys. Rev. Lett.* **34** 953 (1975); Rice T M, Sneddon L *Phys. Rev. Lett.* **47** 689 (1981)
18. Sumi A *J. Phys. Soc. Jpn.* **43** 1286 (1977)
19. Ueta M et al. *Excitonic Processes in Solids* (Springer Ser. in Solid-State Sci., Vol. 60) (Berlin: Springer-Verlag, 1986)
20. Shinozuka Y, Toyozawa Y *J. Phys. Soc. Jpn.* **46** 505 (1979); Toyozawa Y *Physica B + C* **116** 7 (1983)
21. Knox R S *Theory of Excitons* (New York: Academic Press, 1963)
22. Egri I *Phys. Rep.* **119** 363 (1985)
23. Haarer D *Chem. Phys. Lett.* **31** 192 (1975); Haarer D, Philpott M R, Morawitz H *J. Chem. Phys.* **63** 5238 (1975); Elschner A, Weiser G *Chem. Phys.* **98** 465 (1985)
24. Prokof'ev N V, Svistunov B V, Tupitsyn I S *Zh. Eksp. Teor. Fiz.* **114** 570 (1998) [*JETP* **87** 310 (1998)]
25. Prokof'ev N V, Svistunov B V *Phys. Rev. Lett.* **81** 2514 (1998)
26. Mishchenko A S et al. *Phys. Rev. B* **62** 6317 (2000)
27. Mishchenko A S, Nagaosa N *Phys. Rev. Lett.* **86** 4624 (2001)
28. Mishchenko A S, Prokof'ev N V, Svistunov B V *Phys. Rev. B* **64** 033101 (2001)
29. Burovski E A et al. *Phys. Rev. Lett.* **87** 186402 (2001)
30. Mishchenko A S et al. *Nonlinear Opt.* **29** 257 (2002)
31. Mishchenko A S et al. *Phys. Rev. Lett.* **91** 236401 (2003)
32. Mishchenko A S, Nagaosa N *Phys. Rev. Lett.* **93** 036402 (2004)
33. Abrikosov A A, Gor'kov L P, Dzyaloshinskii I E *Metody Kvantovoi Teorii Polya v Statisticheskoi Fizike* (Methods of Quantum Field Theory in Statistical Physics) (Moscow: Dobrosvet, 1998) [Translated into English: *Quantum Field Theoretical Methods in Statistical Physics* 1st ed. (Oxford: Pergamon Press, 1965)]
34. Mahan G D *Many-Particle Physics* 3rd ed. (New York: Kluwer Acad./Plenum Publ., 2000)
35. Jarrell M, Gubernatis J E *Phys. Rep.* **269** 133 (1996)
36. Kress R *Linear Integral Systems* 2nd ed. (New York: Springer-Verlag, 1999)
37. Metropolis N et al. *J. Chem. Phys.* **21** 1087 (1953)
38. Landau D P, Binder K *A Guide to Monte Carlo Simulations in Statistical Physics* (Cambridge: Cambridge Univ. Press, 2000)
39. Sandvik A W, Kurkijärvi J *Phys. Rev. B* **43** 5950 (1991)
40. Tikhonov A N, Arsenin V Y *Solutions of Ill-Posed Problems* (Washington: Winston, 1977); Tikhonov A N, Arsenin V Ya *Metody Resheniya Nekorrektnykh Zadach* 3rd ed. (Methods of Solving Incorrect Problems) (Moscow: Nauka, 1986)
41. Perchik E, math-ph/0302045
42. Phillips D L *J. Assoc. Comput. Mach.* **9** 84 (1962)
43. Tikhonov A N *Dokl. Akad. Nauk SSSR* **151** 501 (1963) [*Sov. Math. Dokl.* **5** 1035 (1963)]
44. Mishchenko A S et al. *Phys. Rev. B* **66** 020301(R) (2002)
45. Aplesnin S S *Zh. Eksp. Teor. Fiz.* **124** 1080 (2003) [*JETP* **97** 969 (2003)]
46. Frenkel J *Phys. Rev.* **37** 17 (1931)
47. Wannier G H *Phys. Rev.* **52** 191 (1937)
48. Onida G, Reining L, Rubio A *Rev. Mod. Phys.* **74** 601 (2002)
49. Albrecht S et al. *Phys. Rev. Lett.* **80** 4510 (1998); Benedict L X, Shirley E L, Bohn R B *Phys. Rev. Lett.* **80** 4514 (1998)
50. Rohlfing M, Louie S G *Phys. Rev. Lett.* **81** 2312 (1998)
51. Marini A, Del Sole R *Phys. Rev. Lett.* **91** 176402 (2003)
52. Devreese J, Evrard R *Phys. Lett.* **11** 278 (1964)
53. Kartheuser E, Evrard R, Devreese J *Phys. Rev. Lett.* **22** 94 (1969)
54. Devreese J, De Sitter J, Goovaerts M *Phys. Rev. B* **5** 2367 (1972)
55. Devreese J T, in *Polarons in Ionic Crystals and Polar Semiconductors* (Ed. J T Devreese) (Amsterdam: North-Holland, 1972) p. 83
56. Mishchenko A S et al., in *Proc. of 2000 Intern. Conf. on Excitonic Processes of Condensed Matter, Osaka, Japan, August 22–25, 2000* (Eds K Cho, A Matsui) (Singapore: World Scientific, 2001) p. 372
57. Lee T D, Low F E, Pines D *Phys. Rev.* **90** 297 (1953)
58. Rashba E I, in *Modern Problems in Condensed Matter Sciences* Vol. 2 (Eds V M Agranovich, A A Maradudin) (Amsterdam: North-Holland, 1982) p. 543; Ioselevich A S, Rashba E I, in *Modern Problems in Condensed Matter Sciences* Vol. 34 (Eds V M Agranovich, A A Maradudin) (Amsterdam: North-Holland, 1992) p. 347
59. Stephan W *Phys. Rev. B* **54** 8981 (1996)
60. Wellein G, Fehske H *Phys. Rev. B* **56** 4513 (1997)
61. Fehske H, Loos J, Wellein G *Z. Phys. B* **104** 619 (1997)
62. Fehske H, Loos J, Wellein G *Phys. Rev. B* **61** 8016 (2000)
63. Bonča J, Trugman S A, Batistić I *Phys. Rev. B* **60** 1633 (1999)
64. Ku L-C, Trugman S A, Bonča J *Phys. Rev. B* **65** 174306 (2002)
65. Shawish S E et al. *Phys. Rev. B* **67** 014301 (2003)
66. Barišić O S *Phys. Rev. B* **65** 144301 (2002)
67. Barišić O S *Phys. Rev. B* **69** 064302 (2004)
68. Sénéchal D, Perez D, Pioro-Landrière M *Phys. Rev. Lett.* **84** 522 (2000); Sénéchal D, Perez D, Plouffe D *Phys. Rev. B* **66** 075129 (2002)
69. Hohenadler M, Aichhorn M, von der Linden W *Phys. Rev. B* **68** 184304 (2003)
70. Gerlach B, Löwen H *Rev. Mod. Phys.* **63** 63 (1991)
71. Pekar S I, Rashba E I, Shcheka V I *Zh. Eksp. Teor. Fiz.* **76** 251 (1979) [*Sov. Phys. JETP* **49** 129 (1979)]
72. Dykman I M, Pekar S I *Dokl. Akad. Nauk SSSR* **83** 825 (1952)
73. Mishchenko A S, Nagaosa N, in *Proc. of 2000 Intern. Conf. on Excitonic Processes of Condensed Matter, Osaka, Japan, August 22–25, 2000* (Eds K Cho, A Matsui) (Singapore: World Scientific, 2001) p. 105
74. Kikoin K A, Mishchenko A S *Zh. Eksp. Teor. Fiz.* **104** 3810 (1993) [*JETP* **77** 828 (1993)]
75. Feynman R P et al. *Phys. Rev.* **127** 1004 (1962)
76. Pitaevskii L P *Zh. Eksp. Teor. Fiz.* **36** 1168 (1959) [*Sov. Phys. JETP* **9** 830 (1959)]
77. Curnoe S, Kikoin K A *Phys. Rev. B* **61** 15714 (2000)
78. Kikoin K A, Mishchenko A S *Zh. Eksp. Teor. Fiz.* **94** (11) 237 (1988) [*Sov. Phys. JETP* **67** 2309 (1988)]
79. Kikoin K A, Mishchenko A S *J. Phys.: Condens. Matter* **2** 6491 (1990)
80. Alekseev P A et al. *Europhys. Lett.* **10** 457 (1989)
81. Mishchenko A S, Kikoin K A *J. Phys.: Condens. Matter* **3** 5937 (1991)
82. Travaglini G, Wachter P *Phys. Rev. B* **29** 893 (1984)
83. Lemmens P et al. *Physica B* **206–207** 371 (1995)
84. Kikoin K A, Mishchenko A S *J. Phys.: Condens. Matter* **7** 307 (1995)
85. Kasuya T *Europhys. Lett.* **26** 277, 283 (1994)
86. Manousakis E *Rev. Mod. Phys.* **63** 1 (1991); Dagotto E *Rev. Mod. Phys.* **66** 763 (1994)
87. Brunner M, Assaad F F, Muramatsu A *Phys. Rev. B* **62** 15480 (2000)
88. Belinicher V I, Chernyshev A L, Shubin V A *Phys. Rev. B* **53** 335 (1996); **54** 14914 (1996)
89. Xiang T, Wheatley J M *Phys. Rev. B* **54** R12653 (1996)
90. Kyung B, Ferrell R A *Phys. Rev. B* **54** 10125 (1996)
91. Lee T K, Shih C T *Phys. Rev. B* **55** 5983 (1997)
92. Lee T K, Ho C-M, Nagaosa N *Phys. Rev. Lett.* **90** 067001 (2003)
93. Tohyama T, Maekawa S *Supercond. Sci. Technol.* **13** R17 (2000)
94. Damascelli A, Hussain Z, Shen Z-X *Rev. Mod. Phys.* **75** 473 (2003)

95. Wells B O et al. *Phys. Rev. Lett.* **74** 964 (1995)
96. Bała J, Oleś A M, Zaanen J *Phys. Rev. B* **52** 4597 (1995)
97. Horsch P, Khaliullin G, in *Open Problems in Strongly Correlated Electron Systems* (NATO Sci. Ser., Ser. II, Vol. 15, Eds J Bonca et al.) (Boston: Kluwer Acad. Publ., 2001) p. 81; Horsch P, Khaliullin G, Oudovenko V *Physica C* **341 – 348** 117 (2000)
98. Rösch O, Gunnarsson O *Phys. Rev. Lett.* **92** 146403 (2004)
99. Rösch O, Gunnarsson O *Phys. Rev. Lett.* **93** 237001 (2004)
100. McQueeney R J et al. *Phys. Rev. B* **54** R9689 (1996); *Phys. Rev. Lett.* **82** 628 (1999); Pintschovius L, Braden M *Phys. Rev. B* **60** R15039 (1999)
101. Hofer J et al. *Phys. Rev. Lett.* **84** 4192 (2000)
102. Bernhard C et al. *Phys. Rev. B* **69** 052502 (2004)
103. Gweon G-H et al. *Nature* **430** 187 (2004)
104. Liu Z, Manousakis E *Phys. Rev. B* **45** 2425 (1992)
105. Ramsak A, Horsch P, Fulde P *Phys. Rev. B* **46** 14305 (1992); Kyung B et al. **54** 13167 (1996); Kyung B, Mukhin S I **55** 3886 (1997)
106. Marsiglio F et al. *Phys. Rev. B* **43** 10882 (1991)
107. Shen K M et al. *Phys. Rev. Lett.* **93** 267002 (2004)
108. Macridin A, Sawatzky G A, Jarrell M *Phys. Rev. B* **69** 245111 (2004)
109. Toyozawa Y *Prog. Theor. Phys.* **26** 29 (1961)